Journal of
Materials Chemistry A

Materials for energy and sustainability

Accepted Manuscript

This article can be cited before page numbers have been issued, to do this please use: M. Gunawan, S. Zhou, D. Gunawan, Q. Zhang, J. N. Hart, R. Amal, J. Scott, N. Valanoor and C. Y. Toe, *J. Mater. Chem. A*, 2025, DOI: 10.1039/D4TA07812H.

ROYAL SOCIETY OF CHEMISTRY

rsc.li/materials-a

View Article Online
DOI: 10.1039/D4TA07812H

Review Article

Ferroelectric materials as photoelectrocatalysts: Photoelectrode design rationale and strategies

Michael Gunawan[1], Shujie Zhou[1], Denny Gunawan[1], Qi Zhang[2,3], Judy N. Hart[2], Rose Amal[1], Jason Scott[1], Nagarajan Valanoor[2]* and Cui Ying Toe[1,4]*

1 Particles and Catalysis Research Group, School of Chemical Engineering, UNSW Sydney, NSW, 2052, Australia

2 School of Materials Science and Engineering, UNSW Sydney, NSW 2052, Australia

3 CSIRO, Manufacturing, Lindfield, NSW 2070, Australia

4 School of Engineering, The University of Newcastle, Callaghan, NSW 2308, Australia

Corresponding authors: nagarajan@unsw.edu.au; cuiying.toe@newcastle.edu.au

Keywords: Ferroelectric, Ferroelectric Polarization, Photoelectrochemical, Photoelectrode, Semiconductor.

ABSTRACT

Ferroelectrics are crystalline materials that possess a permanent and reversible spontaneous polarization. When applied in (opto)electronic devices, the presence of a polarization-induced internal electric field can facilitate enhanced charge separation and transport. Changing the polarization state additionally alters the electronic states and surface properties of ferroelectrics, which can be exploited to gain better control over reaction activity and selectivity when ferroelectrics are used as catalysts. For these reasons, ferroelectrics offer significant potential as new generation photoelectrodes. Given the growing interest in their use for photoelectrochemical applications, it is timely to thoroughly review the intricate

interplay between ferroelectric properties and photoelectrochemical performance. The focus of this review article is to provide such a comprehensive background. We cover the design strategies used thus far for ferroelectric-based photoelectrodes through microstructure tuning, thin film configuration control, and chemical modification through introducing defects and dopants, with a particular focus on factors that impact photoelectrochemical performance. Experimental design considerations for ferroelectric photoelectrodes, including material fabrication, poling methods, and electrolyte selection, which play important roles in ferroelectric-based photoelectrochemical systems, are also highlighted. Ultimately, this review is expected to set the stage for innovative breakthroughs in the design and synthesis of high-performing ferroelectric-based photoelectrodes for sustainable solar fuel and chemical generation.

View Article Online
DOI: 10.1039/D4TA07812H

2. Introduction

The need to find environmentally-friendly and renewable energy options to replace fossil fuels has driven significant advancement in solar energy conversion technologies.[1] Photoelectrochemical (PEC) or photoelectrocatalytic systems have emerged as a promising approach as they exhibit the capacity to capture solar energy during the day and convert it into valuable chemicals or energy carriers that are available to use during both the day-time and night-time.[2,3] PEC systems are relatively simple without expensive solar-to-electricity infrastructure requirements.[4] For example, Shi et al. have demonstrated a PEC system to split water into hydrogen and oxygen with more than 5.7% solar-to-hydrogen conversion efficiency using $BiVO_4$-sensitized mesoporous WO_3/Pt films and a porphyrin-dye-based photoelectrode without any external bias.[5] In recent progress, the application of PEC reactions has been expanded beyond water splitting into producing sustainable platform chemicals. For instance, a PEC system developed by Reisner et al. integrated an alcohol oxidation reaction with a carbon dioxide reduction reaction (CO_2RR) in a tandem PEC configuration.[6] The unique system delivered simultaneous and bias-free aldehyde (value-added chemical) and formate (energy carrier) production under visible-light illumination.

Beyond the traditional semiconductors commonly used in PEC systems, ferroelectric materials, particularly the family of perovskite oxides with the general formula of ABO_3, have attracted much attention.[7-9] Ferroelectrics are a distinct class of materials with non-centrosymmetric crystallographic structures capable of responding to an external electric field.[10] The mismatch between the cation and anion centers of ferroelectric materials generates a dipole moment, known as polarization, which can accelerate charge carrier separation.[11,12] For example, Jiang and co-workers demonstrated a polarization-induced improvement in a $BaTiO_3$ ferroelectric semiconductor on a CdS photoanode. Upon inducing polarization, a 3-fold increase in photocurrent density was observed for PEC water splitting.[13]

View Article Online
DOI: 10.1039/D4TA07812H

Furthermore, the surface adsorption and desorption behavior of ferroelectric materials can be controlled by manipulating their polarization state, improving control over reaction activity and selectivity.[14,15] These unique features of ferroelectric materials make them promising for use as photoelectrodes in PEC cells.

Although ferroelectric materials have shown potential as photoelectrodes, poor light absorption and photoelectrode stability represent primary challenges.[16] Purely ferroelectric photoelectrodes can only deliver photocurrent densities in the order of tens of μA cm^{-2}. Implementing strategies such as oxygen vacancy formation, heterojunction construction, carbon-based material incorporation, and plasmonic element introduction can further advance photocurrent densities to the mA cm^{-2} range.[17-21] These improvements have been associated with a larger range of light absorption, or improved charge separation to prevent self-oxidation and self-reduction.[17-21] Such studies underlie the importance of a thorough understanding on the intrinsic ferroelectric properties of the materials.

While reviews on the utilization of ferroelectric materials in solar harvesting technologies are available,[22-24] there is a notable gap in the discussion of the design principles necessary to construct ferroelectric-based photoelectrodes for various PEC applications. For example, Yu and co-authors described recent advances in ferroelectric materials for PEC applications, while Kim et al. summarized ferroelectric materials employed in PEC systems with an emphasis on water splitting reactions.[23,24] In 2020, Li and co-workers published a review on implementing ferroelectric materials in PEC and photocatalytic water splitting, discussing how the internal electric field can be used to enhance water splitting performance.[22] Understanding the fundamentals of ferroelectrics and PEC is essential to designing ferroelectric-based PEC systems that are high-performing, durable, and scalable. Therefore, a systematic exploration of strategies for designing ferroelectric photoelectrodes, from both PEC and materials viewpoints, is crucial.

The current review offers an in-depth analysis of ferroelectric photoelectrodes for PEC systems, addressing ferroelectric photoelectrocatalyst design strategies and photoelectrocatalytic cell configuration. We begin with an introduction to the general working principles and overview of popular ferroelectric materials for PEC systems (Section 2). This is followed by an in-depth assessment of various design strategies from PEC and materials standpoints, including the effects of: (i) microstructure by tuning of crystallography, orientation and morphology; (ii) thin film configuration control through thickness and/or heterojunction formation; and (iii) chemical and structural modification through doping and/or defect engineering (Section 3). Section 4 addresses the experimental design strategies for ferroelectric photoelectrodes, including fabrication methods, polarization method, and electrolyte selection. Finally, we conclude the review in Section 5 with an outlook and perspective of advancement of PEC systems with ferroelectric photoelectrodes.

3. Ferroelectric materials as photoelectrodes

In the operation of a typical PEC system, there are three major steps involved as shown in **Fig. 1a**: (1) light absorption and photo-induced charge generation; (2) charge transfer and separation; and (3) charge consumption.[25] For the initial step, light is absorbed by a semiconductor with an appropriate bandgap, exciting electrons and producing photogenerated electron-hole pairs, which are then separated. The excited electron migrates to the photocathode, leaving behind a hole which is transferred to the photoanode surface. Ideally, the photogenerated charges are then consumed by reactions on the photoelectrode surfaces. It is essential that the conduction band (CB) and valence band (VB) of the semiconductor have appropriate potentials for the desired reduction and oxidation reactions. For example, in the water splitting reaction, the semiconductor CB must be more negative than the hydrogen

evolution reaction (i.e., the reduction potential of H^+; $E_{CB} < E^0_{red}$), while the VB must be more positive than the water oxidation potential ($E_{VB} > E^0_{ox}$).

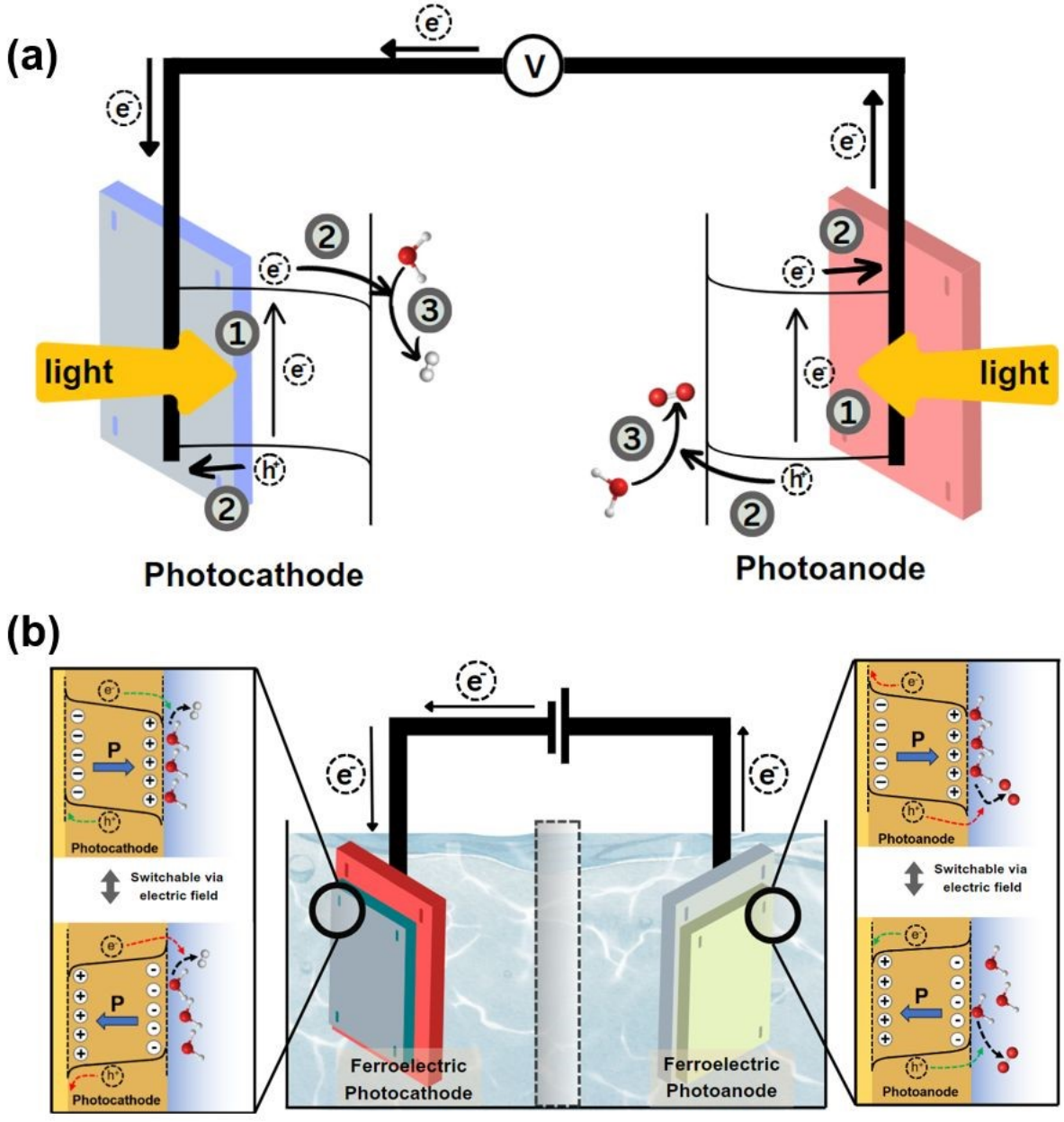

Figure 1. Schematics depicting **(a)** the PEC water splitting mechanism on conventional photoelectrodes which involves three steps: (1) light absorption and charge generation; (2) charge transfer and separation; and (3) charge consumption through surface catalytic reactions; **(b)** The effects on charge transport and water interaction in PEC water splitting due

to poling of ferroelectric photoelectrodes. The colors of the arrows indicate the relative rates of charge transfer, with faster indicated by green and slower by red.

The semiconductor bandgap significantly influences photoelectrode performance as it regulates light spectrum absorption and hence charge generation. A semiconductor material with wide bandgap (wider than 3 eV) is activated only by UV light and is not ideal for solar irradiated-PEC applications. On the other hand, the photovoltage generated by narrow band-gap semiconductors is not sufficient to drive the reactions.[26] Consequently, for a common PEC water splitting application, a bandgap in the range of 1.6–2.6 eV is required to efficiently absorb solar radiation and drive the reactions.[25] Various strategies to engineer the system's light absorption, such as introducing vacancies into the semiconductor, plasmonic doping, and surface modification using photosensitive materials, have been established.[18,20,27-29] For instance, introducing oxygen vacancies by hydrogenating a bismuth ferrite ($BiFeO_3$ / BFO) photoelectrode has been shown to reduce the bandgap from 2.1 eV to 1.9 eV, thereby broadening the light absorption range of the photoelectrode.[30]

Immediately after the charges are generated, it is crucial to swiftly separate and utilize them to minimize charge recombination. At the current developmental stage, electron-hole pair recombination is a significant obstacle in PEC applications.[25] Several key strategies such as shortening the charge migration distance, increasing the charge lifetime, enhancing the conductivity of the semiconductor, and strengthening the driving force for charge separation and migration have been explored to suppress charge recombination.[31] These approaches are implemented by modifying the photoelectrodes by nanostructure engineering, introduction of dopants, crystal facet engineering, and formation of heterojunctions.[32-39]

View Article Online
DOI: 10.1039/D4TA07812H

Ultimately, the photogenerated electrons and holes should be consumed for reduction and oxidation reactions at the surfaces of the (photo)cathode and (photo)anode, respectively. At this step, the reaction kinetics, including the adsorption and/or desorption of the reactants and/or products play a determining role in the efficiency and selectivity of the reactions.[40] Several reviews have addressed how these critical steps can be promoted for conventional photoelectrode systems, such as by introducing surface passivation layers,[41] improving charge dynamics,[42] introducing co-catalysts,[43] and employing alternative reactions.[44]

Various ferroelectrics have been implemented as photoelectrodes for different PEC applications, as summarized in **Table 1**.[45-48] Among these, titanates (e.g., $PbTiO_3$ / PTO and $BaTiO_3$ / BTO) are the most widely studied ferroelectric materials as photoelectrodes, followed by the group of ferrites, which is dominated by $BiFeO_3$. The increased interest in ferroelectric photoelectrodes can be attributed to their permanent and reversible intrinsic electric polarization upon exposure to an external electric field, which can improve PEC performance particularly by facilitating photo-induced charge separation and suppressing charge recombination,[11] hence potentially overcoming one of the main limiting factors in current PEC systems. As depicted in **Fig. 1b**, switching the polarization state of a ferroelectric material induces the displacement of charged ions within the material, leading to a non-neutral surface charge. The charged surface generates an electric field at the semiconductor-electrolyte interface (SEI) and across the whole ferroelectric layer which will affect the rate of charge transfer to the surface and/or the conductive substrate. Moreover, the two distinct surfaces of ferroelectric materials in different polarization states could tailor the adsorption strengths of reactants and products, allowing enhanced activity as well as better control over the selectivity of the products.[49-53]

Many studies have demonstrated these features of ferroelectric photoelectrodes in PEC reactions.[17,19,51,54-56] For example, Augurio et al. demonstrated that ferroelectric polarization

View Article Online
DOI: 10.1039/D4TA07812H

can enhance PEC performance of a $BaTiO_3$ photoanode.[51] The enhanced PEC performance was attributed to band bending at the $BaTiO_3$/electrolyte interface which facilitated faster charge separation. In the case of controlling the adsorption strength, an In_2Se_3 monolayer has been shown to exhibit reversible chemical-physical adsorption by ferroelectric switching, demonstrating the potential for controlling catalytic reactions through polarization changes.[57] The polarization-dependence of adsorption strength has also been shown on oppositely poled $LiNbO_3$ surfaces – on a positively-charged $LiNbO_3$ surface, the peak desorption temperature for acetic acid was observed to be 100 K higher compared to the negatively-charged surface.[58] Further, the interactions of H_2O and CH_3OH with $LiNbO_3$ were influenced by the polarization direction, demonstrating the potential realization of tunable catalytic reactions on the ferroelectric surface.[59]

The unique phenomenon of polarization-induced surface reconstruction particularly opens avenues for designing cyclic catalytic pathways in PEC and related applications, both for liquid- and gas-state adsorbates. An intriguing example comes from the work by Kakekhani, who developed a model for catalytic NO_x decomposition and water splitting over a $PbTiO_3$-based catalyst.[14,15] By cyclically switching the polarization, it was predicted that variations in the thermodynamically stable surface termination could be harnessed to drive desired reactions, as depicted in **Fig. 2**. The findings illustrate the potential of ferroelectric materials to revolutionize catalytic processes.

View Article Online
DOI: 10.1039/D4TA07812H

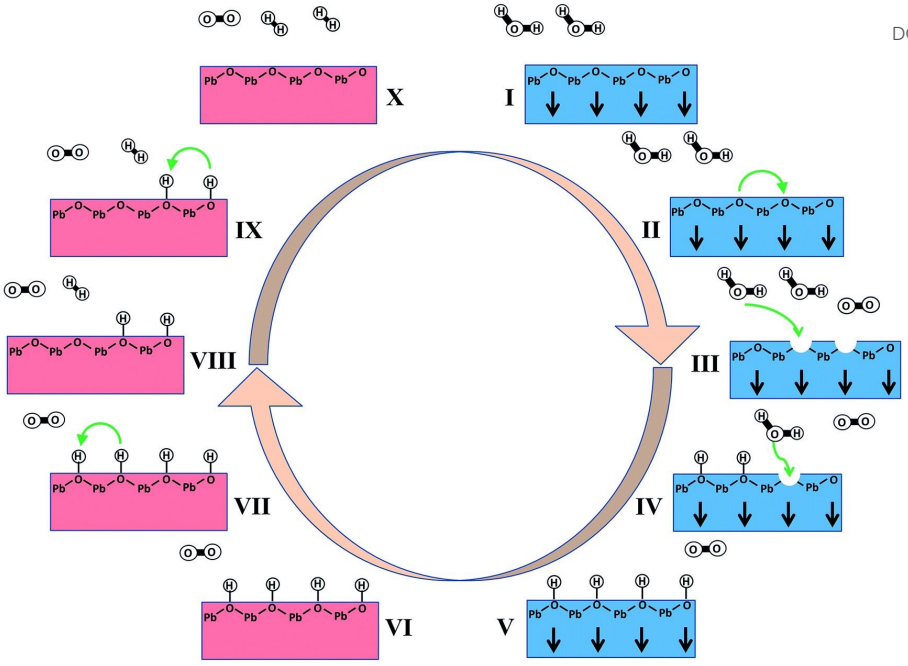

Figure 2. Schematic of proposed water splitting reaction by cyclic switching between the negatively poled and paraelectric (001) surface of $PbTiO_3$. Two H_2O molecules are adsorbed and dissociated on the negatively poled surface to produce bound atomic H. When the surface is switched to the paraelectric phase, the H atoms recombine to form weakly bound H_2, creating a pristine surface ready for the next cycle. Reproduced with permission.[14] Copyright 2016, Royal Society of Chemistry.

The early development of ferroelectric photoelectrodes was dominated by lead titanate ($PbTiO_3$), which has a space group of *P4-mm* and Curie temperature (T_C) of 495 °C.[60] One of the earliest studies reported fabrication of a $PbTiO_3$-PbO composite photoelectrode from a mixture of PbO_2 and TiO_2 which had undergone solid-state sintering.[61] Given the infancy of its development at the time, single-phase $PbTiO_3$ was not achievable, with PbO also being present. Nevertheless, the early $PbTiO_3$-PbO photoelectrode exhibited impressive PEC performance with an open-circuit potential (V_{oc}) of 0.38 V and solar-to-electrical conversion efficiency of 0.04% under 100 mW cm^{-2} white-light illumination. Single-phase $PbTiO_3$ has

View Article Online
DOI: 10.1039/D4TA07812H

since been successfully synthesized by various methods, including hydrothermal and chemical ripening processes using TiO_2 and PbO precursors.[62,63] It has consequently been shown that the spontaneous polarization of $PbTiO_3$ produces polarization-dependent band bending that suppresses electron-hole pair recombination, thus enhancing PEC performance.[63-69] However concern regarding lead toxicity has seen the attractiveness of $PbTiO_3$ by the PEC community diminish, leading to interest in other metal-oxide ferroelectric materials.

Thus, as a lead-free alternative, barium titanate ($BaTiO_3$) has emerged as a popular photoelectrode. In addition to the environmental and health issues, the absence of lead makes $BaTiO_3$ more robust compared to $PbTiO_3$ as it is free from the issues of high vapor pressure and lead volatility, ensuring stable stoichiometry, better mechanical stability, and long-term reliability.[70] Moreover, $BaTiO_3$ has a T_C of 120 °C, which is still within the operation range of PEC applications (normally lies below 100 °C). $BaTiO_3$ has exhibited great potential for PEC systems due to its beneficial characteristics including appropriate band positions, abundant oxygen vacancies, tunable particle size and morphology, robust spontaneous polarization, rapid migration of photogenerated charge carriers, and band bending.[16,37,48,51,71-74] Despite these advantages, the large bandgap of $BaTiO_3$ (3.2 eV) means it captures less than 5% of solar photons due to its narrow absorption capability, limiting its application as a photoelectrode for PEC solar conversion.[16]

Beyond $PbTiO_3$ and $BaTiO_3$, BFO has recently received significant attention over the past decade due to its bandgap (2.3–2.7 eV) being more appropriate for solar harvesting. Additionally, its suitable band position for the hydrogen evolution reaction (HER), non-toxic nature, and earth-abundant metal constituents make BFO promising for PEC applications. Huang et al. reported a remnant polarization (P_r) value of ~84.9 μC.cm^{-2} for BFO, which results in a strong polarization electric field and hence good band bending and charge

View Article Online
DOI: 10.1039/D4TA07812H

separation during the PEC process.[75] However, BFO is reported to suffer from large current leakage. In a PEC system, current leakage can accelerate photoelectrode depolarization, leading to poor photoelectrode stability and progressive loss in performance.[76] Strategies have been implemented to address this issue including elemental doping and defect engineering.[27,77-80]

Other commonly studied ferroelectric photoelectrodes include alkali niobates ($NaNbO_3$, $LiNbO_3$, $KNbO_3$) and tantalates ($NaTaO_3$, $LiTaO_3$, $KTaO_3$). The niobates and tantalates have been attracting attention as PEC electrode materials as they are lead-free and exhibit outstanding ferroelectricity originating from distortion of [NbO_6] or [TaO_6] octahedra. [35,81-83] Also, for tantalates, the Ta−O−Ta bond angles are reported to assist in delocalizing the excited energy to facilitate catalytic reactions.[84]

As mentioned earlier, to employ ferroelectric materials as photoelectrodes, the optical, electronic, and ferroelectric properties of the materials need to be initially screened. Important parameters including the saturation polarization intensity (P_s), the remnant polarization intensity (P_r) and the coercive field (E_c) can be deduced from the polarization strength-electrical field (*P*–*E*) loops, as shown in **Fig. 3a**.[85] These parameters and the shape of the hysteresis loop are important to define the performance of ferroelectric materials and devices. Generally, a larger remnant polarization value is better as it indicates stronger polarization remaining within the material after the electric field is removed. Coercive field indicates the strength of the electric field at which the macroscopic polarization disappears, with higher values being preferred.

From the semiconductor standpoint, the material should have a suitable bandgap that facilitates solar light absorption (ideally around 1.6 – 2.6 eV for water splitting applications). As shown in **Fig. 3b**, the wider the bandgap, the lower the theoretical photocurrent density,

and the lower the solar-to-hydrogen conversion efficiency. The electronic band positions (**Fig. 3c**) of the photoelectrode must be evaluated against the standard redox potentials of the reactions involved. Assignment of a ferroelectric semiconductor as a photocathode or photoanode could be justified by comparing the band-edge positions against the standard redox potentials of the targeted reactions (e.g., 0 V vs. NHE for HER and 1.23 V vs. NHE for water oxidation, OER). The intrinsic semiconducting type of each material also requires consideration when assigning a ferroelectric material as a photocathode or photoanode – an n-type semiconductor is usually employed as a photoanode and a p-type semiconductor as a photocathode.

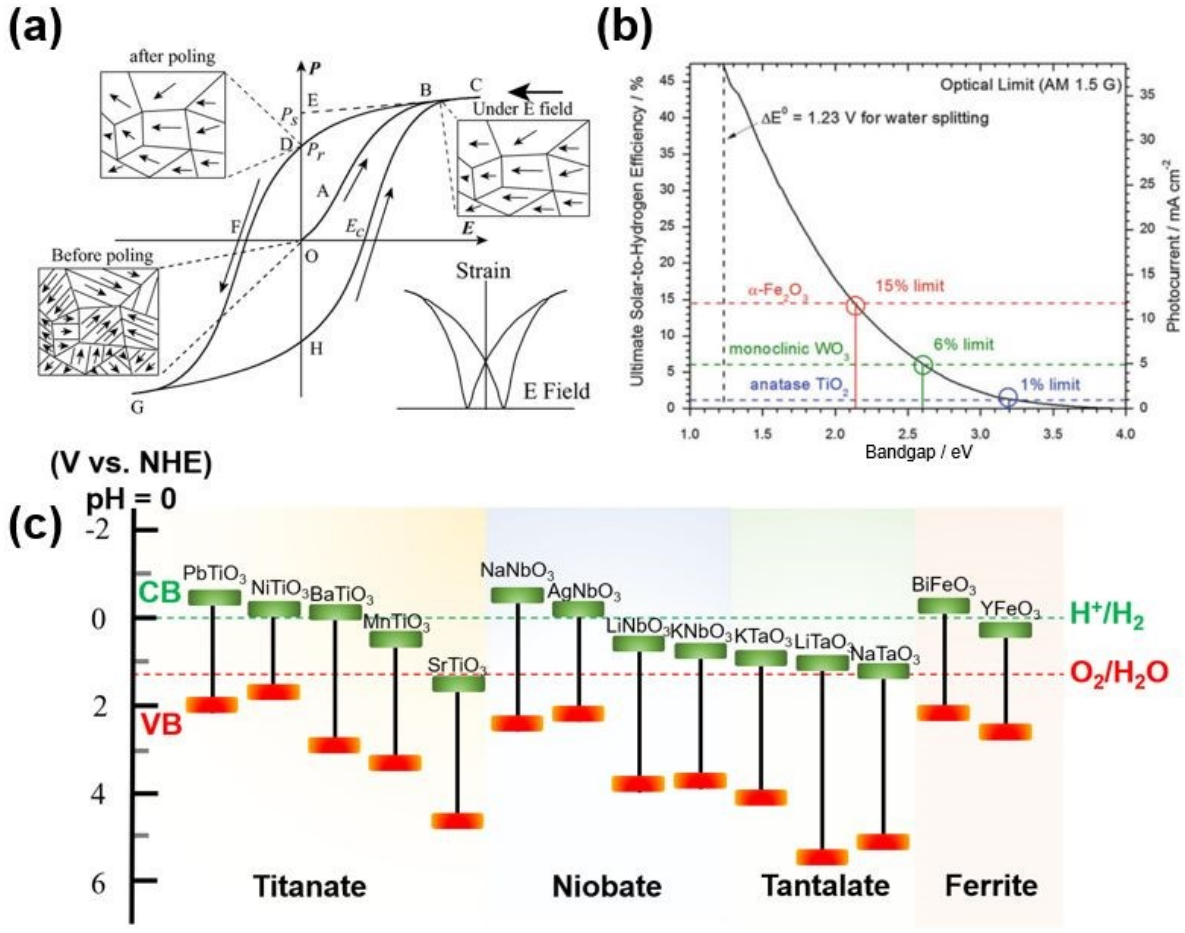

Figure 3. (a) Typical hysteresis loop of a ferroelectric material, with corresponding domain reversal (polarization rotation) state and strain–electric field curve. Reproduced with

permission.[86] Copyright © 2013, John Wiley and Sons. **(b)** Theoretical maximum solar-to-hydrogen (STH) conversion efficiency (left axis) and photocurrent (right axis) as a function of material bandgap. Reproduced with permission.[87] Copyright © 2013, The Authors, published by Springer. **(c)** Band edge positions of different ferroelectric semiconductors used in water splitting.

4. Design Strategies for Ferroelectric Photoelectrodes

The capability of ferroelectric-based photoelectrodes in enhancing charge separation and controlling reaction selectivity for PEC applications has been proven. Nevertheless, bare ferroelectric materials have so far exhibited very low photocurrents due to their wide bandgaps and substantial defect-induced current leakage. The next section of the review outlines essential design strategies for ferroelectric-based photoelectrodes, including microstructure tuning, thin film configuration design, and chemical modification, to provide future directions to enhance the PEC performance of ferroelectric photoelectrodes. Collectively, the strategies contribute to developing high-performance ferroelectric-based photoelectrodes for PEC applications.

3.1.Microstructure Tuning

The properties of ferroelectric materials strongly depend on their crystallographic microstructure, especially on the crystal growth orientation. Polycrystalline ferroelectric materials present polydomain structures where oppositely aligned domains may reduce the net polarization and hence nullify the ferroelectric enhancement in most cases.[88] This effect will also lead to higher charge recombination in a polycrystalline ferroelectric compared to a single-crystal ferroelectric.[89] Therefore, it is generally preferable to use single-crystal materials. He et al. successfully tuned the crystallinity of BFO from polydomain to single

View Article Online
DOI: 10.1039/D4TA07812H

domain by changing the precursor solvent and hydrothermal treatment time during synthesis.[88] Photogenerated electrons and holes in the single-domain BFO were efficiently separated and transferred to the positive and negative polarization surfaces, respectively, invoking a nine-fold increase in photocatalytic water oxidation under visible-light irradiation, compared to polydomain BFO particles. The most common method to grow single-crystal ferroelectrics involves using a template with a specific orientation. Our research group adopted this strategy with a chemical solution deposition method to fabricate epitaxial (001) BFO thin films on a strontium titanate ($SrTiO_3$, STO) (001) substrate.[90] The approach produced well-oriented BFO films with excellent ferroelectric properties where no secondary phase formation was observed.

Beyond crystal uniformity, polarization in different crystal orientations introduces changes in the optical, electronic and ferroelectric properties of ferroelectric semiconductors. Song et al. demonstrated these effects by observing the PEC performance of BFO photoelectrodes with different crystallographic orientations.[80] As shown in **Fig. 4a**, the different crystallographic orientations affected the conduction and valence bands of BFO, with almost 0.2 eV difference between $(001)_{pc}$ and $(111)_{pc}$. Among $(111)_{pc}$, $(001)_{pc}$, and $(110)_{pc}$ oriented epitaxial BFO domains, $(111)_{pc}$ exhibited superior performance with a photocurrent density of 0.046 mA cm^{-2} at 0 $V_{Ag/AgCl}$. Notably, the $(111)_{pc}$ oriented BFO featured a bandgap of 2.57 eV and an onset potential of -0.382 $V_{Ag/AgCl}$, which was lower than for $(001)_{pc}$ and $(110)_{pc}$. In addition to changing the band positions, different crystallographic orientations were shown to affect the P_r value (**Fig. 4b-c**), resulting in different intensity of band bending at the SEI (illustrated in **Fig. 4d**). The higher P_r value of $(111)_{pc}$ resulted in the strongest downward band bending in down-poled BFO amongst the three orientations, delivering the greatest enhancement in PEC performance for the down-poled case (0.08 mA cm^{-2} at 0 $V_{Ag/AgCl}$).

View Article Online
DOI: 10.1039/D4TA07812H

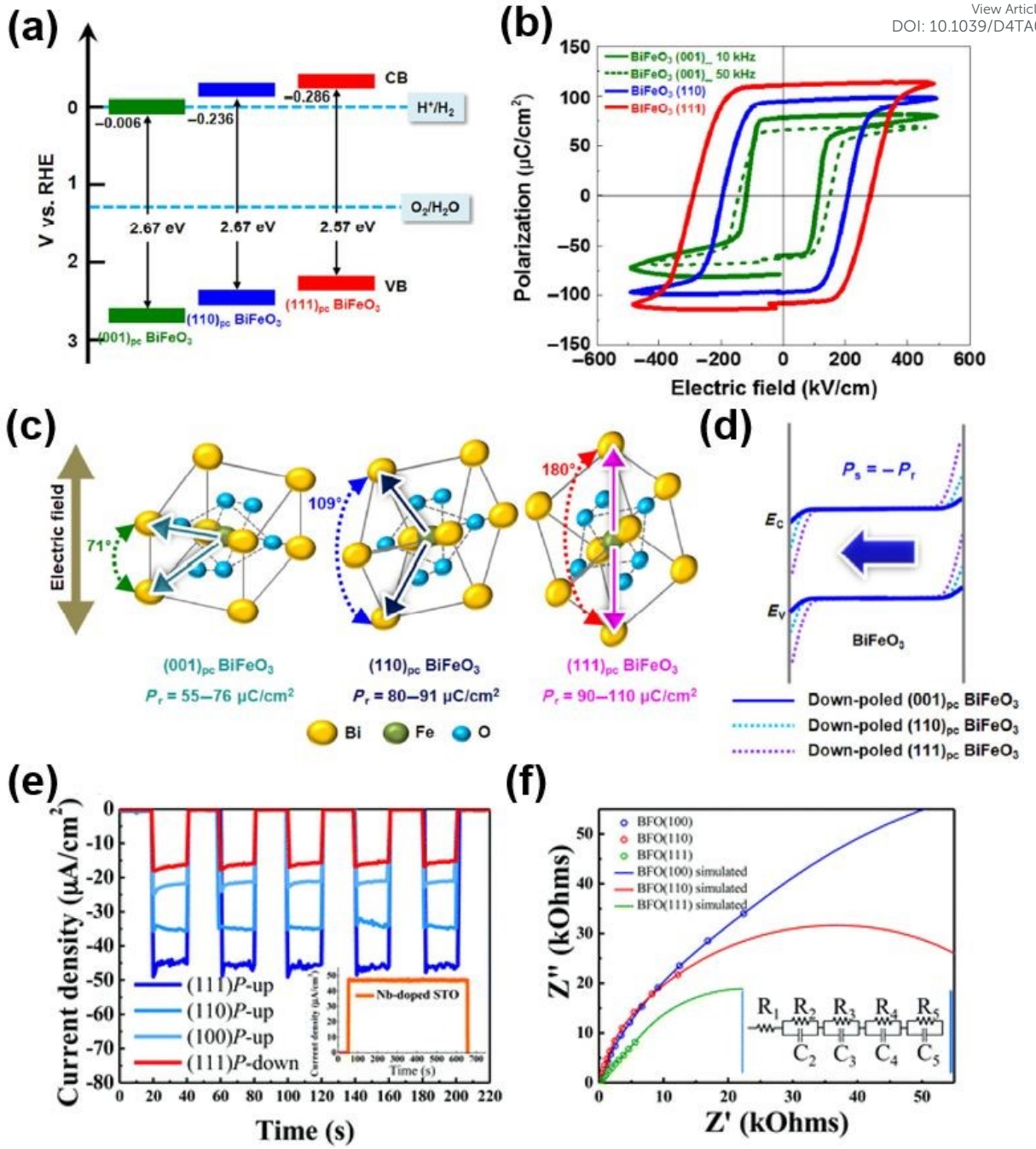

Figure 4. **(a)** Band positions, **(b)** *P*–*E* hysteresis loop measurements, **(c)** ferroelectric polarization paths and P_r values, and **(d)** band energy diagram for $BiFeO_3$ thin-film photoanodes with different crystallographic orientations. Reproduced with permission.[80] Copyright © 2017, Springer Nature. **(e)** Photocurrent measurements under zero bias (0 V *vs.*, Ag/AgCl) and **(f)** electrochemical impedance spectroscopic analysis of the three different

View Article Online
DOI: 10.1039/D4TA07812H

orientations of BFO thin films. Reproduced with permission.[75] Copyright 2016, Royal Society of Chemistry.

Similarly, Huang et al. investigated Au/BFO with different orientations synthesized by pulsed laser deposition (PLD) on a single-crystal (0.5 wt%) Nb-doped STO substrate with (100), (110), and (111) orientations.[75] As shown in **Fig. 4e**, up-poled $BFO_{(111)}$ exhibited the best PEC performance (45 μA cm^{-2}) at 0 $V_{Ag/AgCl}$, followed by $BFO_{(110)}$ (35 μA cm^{-2}) and $BFO_{(100)}$ (25 μA cm^{-2}) under the same measurement conditions. This superior performance by $BFO_{(111)}$ was attributed to: (i) a higher valence band position providing more carriers to participate in the water splitting process and reducing charge transfer resistance, and (ii) higher spontaneous polarization along the [111] direction providing a higher driving force for charge separation as indicated by the smaller radius in the Nyquist plot obtained from electrochemical impedance spectroscopy (**Fig. 4f**).

The direction of crystal growth also affects the crystal facets exposed on which the catalytic reactions occur.[91,92] Due to anisotropy of the crystal planes, some ferroelectric metal oxides exhibit facet-dependent physical and chemical properties. This includes geometric structures, surface electronic structures, surface built-in electric fields, and redox active sites, which create differences in the adsorption energies of oxygen or hydrogen intermediates, leading to different HER or OER PEC activities.[91,93,94] Ferroelectric monoclinic $KNbO_3$ nanowires (m-$KNbO_3$ NWs) exposing {100}, {010} and {001} facets with a growth direction of [100], and orthorhombic (o-$KNbO_3$) NWs enclosed by {101} and {010} facets with a growth direction of [101], possess bandgaps of 3.15 eV and 3.25 eV, respectively.[95] As expected, the different $KNbO_3$ NW structures exhibited different P_r values. The $<10\bar{1}>$ direction for m-$KNbO_3$ gave a P_r value of 20 μC.cm^{-2} while the <001> direction for o-$KNbO_3$ gave a P_r value of 42 μC.cm^{-2}. The higher P_r value of o-$KNbO_3$ indicates a stronger ferroelectric-induced electrical

View Article Online
DOI: 10.1039/D4TA07812H

field held by the materials. The enhanced ferroelectric properties, as well as the more energetic conduction band of o-$KNbO_3$, meant the photoactivity of the o-$KNbO_3$ NWs was up to two-fold greater than m-$KNbO_3$ under identical experimental conditions.

The above demonstrates that the design and morphological control of crystal facets and surface atomic arrangement in ferroelectric-based photoelectrodes is crucial for optimal performance. Based on the Gibbs-Wulff theory, semiconductor crystals formed under equilibrium conditions tend to expose less reactive (low-energy) facets,[91] but these facets are not desirable in terms of PEC activity. To address this, various strategies can be employed to facilitate tailored tuning of the exposed facets. This includes altering the synthesis method, adjusting the annealing temperature, using different solvents and introducing capping agents.

To produce BFO with distinct facets, Djatoubai and co-workers varied the NaOH concentration during a hydrothermal synthesis process.[33] Varying the NaOH concentration led to different BFO morphologies, attributed to the agglomeration of BFO nanoparticles in a specific direction. A higher NaOH concentration (12.5 M) produced BFO nanoplates, while lower concentrations (8 M and 3.5 M) yielded rectangular cuboids and hexagons, respectively. Notably, the rectangular cuboid BFO, dominated by (102) crystal facets, exhibited efficient charge carrier separation compared to the hexagons with (102) facets and nanoplates with (104) facets, resulting in enhanced water splitting performance by the BFO rectangular cuboids (higher oxygen gas yield by ~1.93 and ~1.55 times compared to the BFO hexagons and nanoplates, respectively).

While facet engineering is one of the most explored strategies in PEC in general, its application to ferroelectric photoelectrodes remains limited. Subsequently, a distinct opportunity is available to explore facet engineering as a strategy to promote ferroelectric

View Article Online
DOI: 10.1039/D4TA07812H

performance and establish the correlation between exposed facet and ferroelectric semiconductor behavior.

3.2. Thin Film Configuration Control

3.2.1. Thickness

Semiconductor film thickness can significantly affect ferroelectric properties, light absorption, and charge separation beahvior of photoelectrodes. The optimum thickness of a ferroelectric photoelectrode will be attained when all ferroelectric properties, photoactivity, and charge transfer efficiency are considered. One effect that is particularly important in ferroelectric thin films is the substrate clamping effect.[96-98] When a ferroelectric layer is grown on a substrate, part of the ferroelectric layer is clamped due to lattice mismatch between the substrate and the ferroelectric layer. As the film thickness decreases, a larger proportion of the film is influenced by the clamping effect, resulting in stronger domain wall pinning and a higher driving electric field required to achieve a uniform polarization state.[99] For instance, Pérez de la Cruz et al. explored the influence of substrate clamping on the microscopic piezoelectric response of lead zirconate titanate (PZT) as the film thickness decreased.[100] PZT thin films with varying thicknesses were deposited on $Pt_{(111)}$/Ti/SiO_2/Si substrates using a sol-gel method. They reported that 140 nm-thick films exhibited a single perovskite phase with (111) texture. As the film thickness increased to 420 and 700 nm, the films transitioned into a highly (100)-oriented state, accompanied by an increase in the mean grain size. The changes had a direct impact on the dielectric permittivity (ε) of the PZT films, which steadily increased from 848 (for the 140 nm thick PZT film) to 1270 (for the 700 nm thick PZT film).

To efficiently capture the solar spectrum, the choice of thickness of the semiconductor absorber layer must consider the incident light penetration depth, which is inversely related to

View Article Online
DOI: 10.1039/D4TA07812H

the absorption coefficient. Further, thick semiconductor films mean longer migration lengths for the photoexcited charges, which leads to a higher probability of photo-generated charge recombination.[26] There is typically an optimum thickness for every photoelectrode type. Photoelectrodes with a thickness beyond the optimum point can suffer from high charge recombination. For example, Haydous et al. demonstrated that epitaxial yttrium-doped bismuth ferrite ($Bi_{0.97}Y_{0.03}FeO_3$) films grown on a (001) Nb-doped STO substrate by PLD exhibited PEC properties with a strong dependence on film thickness (**Fig. 5a**).[36] A film thickness of 22 nm produced a photocurrent of 0.72 mA cm^{-2} at 1.4 V_{RHE}, twelve times higher than the photocurrent density exhibited by a 75 nm-thick film (0.06 mA cm^{-2} at 1.4 V_{RHE}) under the same illumination and testing conditions (**Fig. 5b**). The thicker film was reported to invoke a higher charge recombination rate which was detrimental to PEC performance.

Others have reported on optimum thicknesses for various ferroelectric-based photoelectrodes, including BFO[36,101,102], BTO[103], and PTO[103], which exhibit good ferroelectric properties and PEC performance. A study by Liu et al. highlighted the importance of finding the optimum thickness of ferroelectric-based photoelectrodes.[104] A polycrystalline BFO thin film on a $Pt/Ti/SiO_2/Si_{(100)}$ substrate was found to experience a bandgap decrease from 2.46 eV to 2.32 eV with increasing film thickness from 160 nm to 280 nm, arising from improved crystallinity of the thicker samples (**Fig. 5c**). Additionally, based on UV-vis spectra, light absorbance by the photoelectrode was enhanced in both the UV and visible-light regions for the thicker films. PEC testing (**Fig. 5d**) demonstrated that 200 nm BFO gave a higher photocurrent magnitude (-15 μA cm^{-2} at 0 V vs RHE) compared to 160 nm BFO (-7 μA cm^{-2} at 0 V vs RHE). A further increase in film thickness (240 and 280 nm) deteriorated the PEC performance due to severe charge recombination in the bulk of the photoelectrode. The above findings underscore the critical role thickness plays in regulating the ferroelectric properties

View Article Online
DOI: 10.1039/D4TA07812H

and PEC performance of ferroelectric-based photoelectrodes. Thus, studies of ferroelectric photoelectrodes should pay attention to the thickness used, and the development of film fabrication methods with controllable and uniform thickness should be explored.

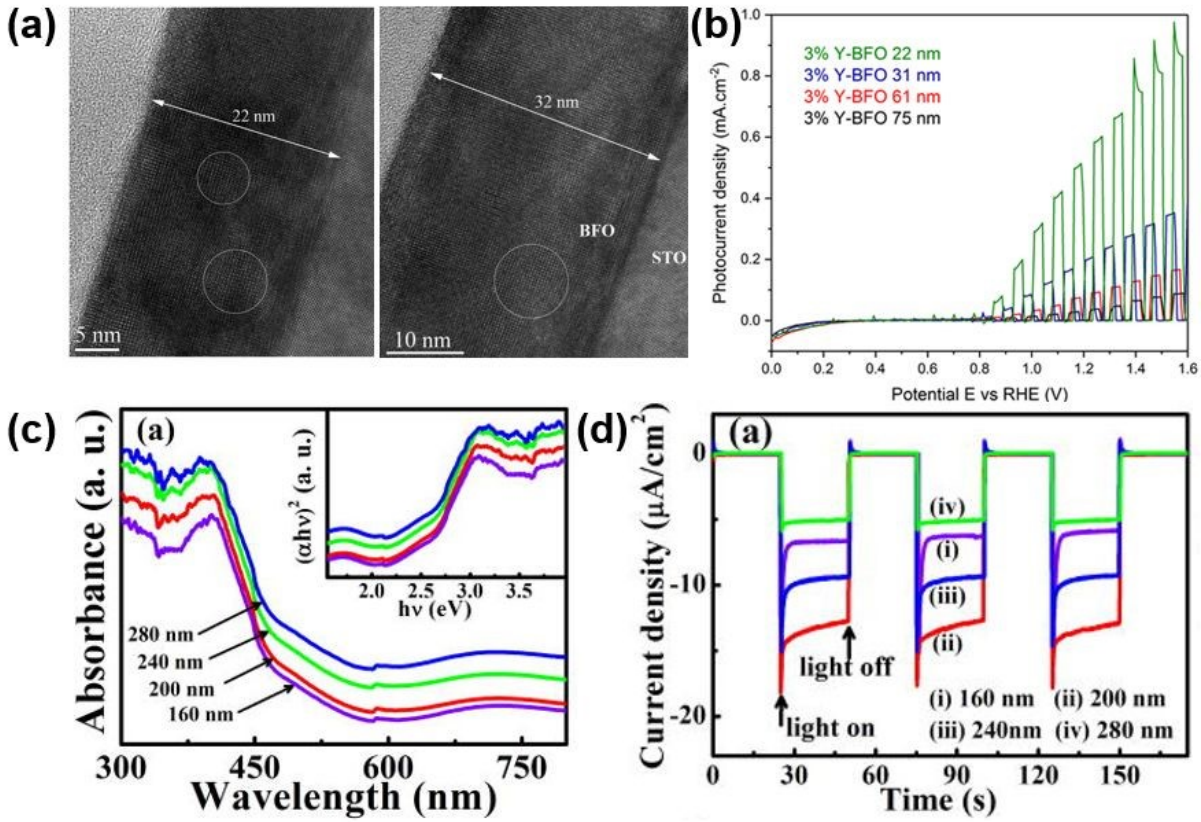

Figure 5. High resolution transmission electron microscopy (HRTEM) cross-sectional images of yttrium-doped bismuth ferrite ($Bi_{0.97}Y_{0.03}FeO_3$, Y-BFO) films with thicknesses of **(a)** 22 nm and 32 nm, **(b)** potentiodynamic measurements for the Y-BFO thin films. Reproduced under terms of the CC-BY license.[36] Copyright © 2018, The Authors, published by Springer Nature. **(c)** UV-vis absorption spectra and optical bandgaps (inset), and **(d)** photocurrent densities *versus* time (measured under intermittent light illumination) of BFO films with different thicknesses. Reproduced with permission.[104] Copyright 2016, AIP Publishing.

View Article Online
DOI: 10.1039/D4TA07812H

3.2.2. Heterojunctions

A heterojunction is defined as the interfacial contact between two semiconductors with different crystallographic properties and band structures, which can result in a built-in electrical field to accelerate charge separation.[105] Designing a photoelectrode based on a heterojunction with an appropriate band alignment allows for efficient charge injection from one semiconductor to the other, facilitating charge separation and prolonging charge lifetimes compared with the use of single materials.[26] Beyond charge separation, heterojunction engineering has also been widely implemented to improve light absorption, since heterojunctions can allow absorption of a greater portion of the light spectrum than single materials due to differences in the bandgaps of the two semiconductors in the heterostructure.[26,106]

Combining a ferroelectric material with an excellent light-absorbing semiconductor can be beneficial as utilization of a significant portion of the solar spectrum is then enabled. For instance, by combining BFO with Sn-doped TiO_2, Huang et al. achieved a photocurrent density of 1.76 mA cm^{-2} at 1.23V vs. RHE, higher than the photocurrent for Sn-doped TiO_2 (0.84 mA cm^{-2}) and neat BFO (typically in the order of μA cm^{-2}).[107] When designing a heterojunction for a PEC photoelectrode, achieving a proper band-edge alignment at the interface is crucial for maximally exploiting the heterojunction effect to enhance charge transfer.[108] Heterojunction configurations, as illustrated in **Fig. 6(a-b)**, include type-I and type-II heterostructures. The type-I heterostructure consists of a semiconductor with more negative CB and more positive VB (Semiconductor A) and a semiconductor with less negative CB and less positive VB (Semiconductor B). As a result, both electrons and holes are transferred from A to B. This type of heterojunction is rarely implemented in PEC systems as the photoexcited electrons and holes in a PEC system should be guided in opposite directions to promote spatial charge separation.

View Article Online
DOI: 10.1039/D4TA07812H

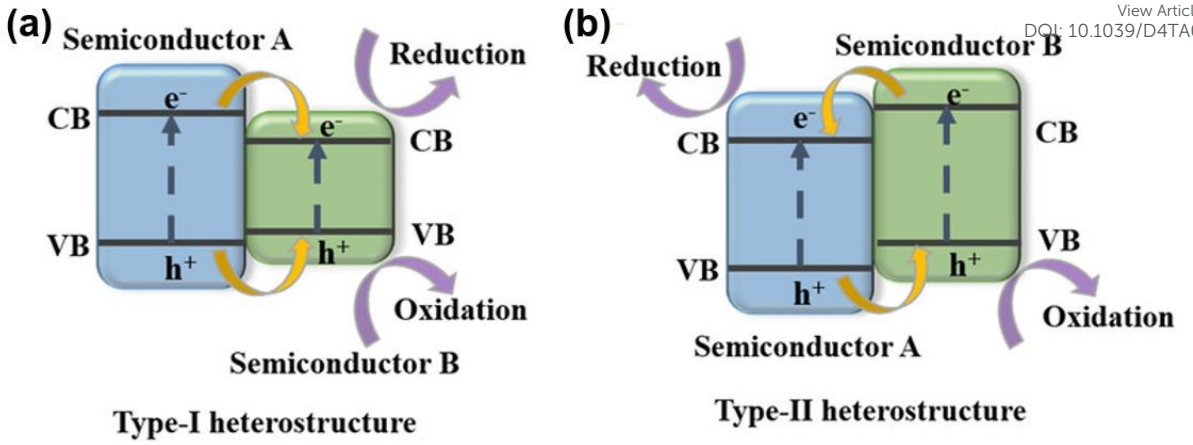

Figure 6. Different heterojunction types for photoelectrodes, with their band alignments and the possible mechanisms of charge transfer indicated: **(a)** type-I heterojunction and **(b)** type-II heterojunction. Reproduced under terms of the CC-BY license.[109] Copyright © 2022, The Authors, published by Wiley-VCH GmbH.

In contrast, a type-II heterostructure involves a semiconductor with less negative CB and more positive VB (Semiconductor A) and a semiconductor with more negative CB and less positive VB (Semiconductor B). This configuration allows the photogenerated electrons in Semiconductor B to be transferred to Semiconductor A, while the photogenerated holes in Semiconductor A are transferred to Semiconductor B, realizing spatial charge separation. This heterojunction is the most common applied in PEC systems as it provides an additional driving force for photogenerated charge separation.[109]

As widely reported, changes in the polarization direction in ferroelectric materials can alter the band positions of the materials.[110] In photosensing device development based on heterojunctions, ferroelectric polarization-induced band-engineering has successfully tuned the nature of the heterojunction formed and thus changed the carrier transport mechanism. For example, Chen et al. synthesized a type-II heterojunction by integrating ferroelectric germanium monoselenide (GeSe) and molybdenum sulfide (MoS_2).[111] Transition of the

View Article Online
DOI: 10.1039/D4TA07812H

heterojunction from type-II to type-I was realized by switching the polarization state to the downward state. This phenomenon was attributed to the polarization shifting the conduction band position of GeSe to a more negative potential, thus changing it from being higher to lower relative to the conduction band of MoS_2, thus a type-I (straddling) band alignment was formed. This unique ability could be beneficial for photoelectrochemical systems by altering straddling type heterojunctions (type-I) to staggered gap heterojunctions (type-II).

A commonly-reported ferroelectric material used in heterojunctions is BTO, often coupled with a high-performance PEC material.[71,72,112] The heterojunction improves overall PEC efficiency due to the strong ferroelectric polarization of the BTO crystals. A notable example is TiO_2/BTO core/shell NWs synthesized using a two-step hydrothermal process.[72] Interestingly, the thickness of ferroelectric materials is important not only for the standalone ferroelectric materials (as discussed in section 3.2.1.) but also for heterostructures. The TiO_2/BTO core/shell NWs with 5 nm BTO thickness yielded significantly higher photocurrent densities (1.30 mA cm^{-2} at 1.23 V_{RHE}) compared to bare TiO_2 (0.78 mA cm^{-2} at 1.23 V_{RHE}). When the BTO thickness was increased to 40 nm, the photocurrent density dropped to 0.74 mA cm^{-2} at 1.23 V_{RHE} due to a higher bulk recombination rate in the thick BTO shells. Positive poling resulted in enhanced photocurrent density for TiO_2/BTO-5nm but decreased the performance of TiO_2/BTO-40nm (**Fig. 7a-b**), while the opposite trend was seen for negative poling, i.e. poling decreased PEC performance for TiO_2/BTO-5nm but enhanced it for TiO_2/BTO-40nm. As schematically shown in **Fig. 7c-d**, the internal electric field induced in BTO by negative polarization accelerates the transport of holes to the BTO/NaOH interface. In contrast, positive poling induces an unfavorable gradient in the BTO valence band, which impedes the charge transfer to the BTO/NaOH interface but enhances band bending and hence the width of the depletion region in the TiO_2. For thethicker BTO (TiO_2/BTO-40nm), the effect of polarization on transport across the BTO layer and to the

BTO/NaOH interface dominates, such that the best performance is seen with negative poling, but for the thin BTO (TiO_2/BTO-5nm) holes can tunnel through the BTO shell, so the band alignment in the BTO shell is less significant and the effect of polarization is dominated by the band bending in the TiO_2.

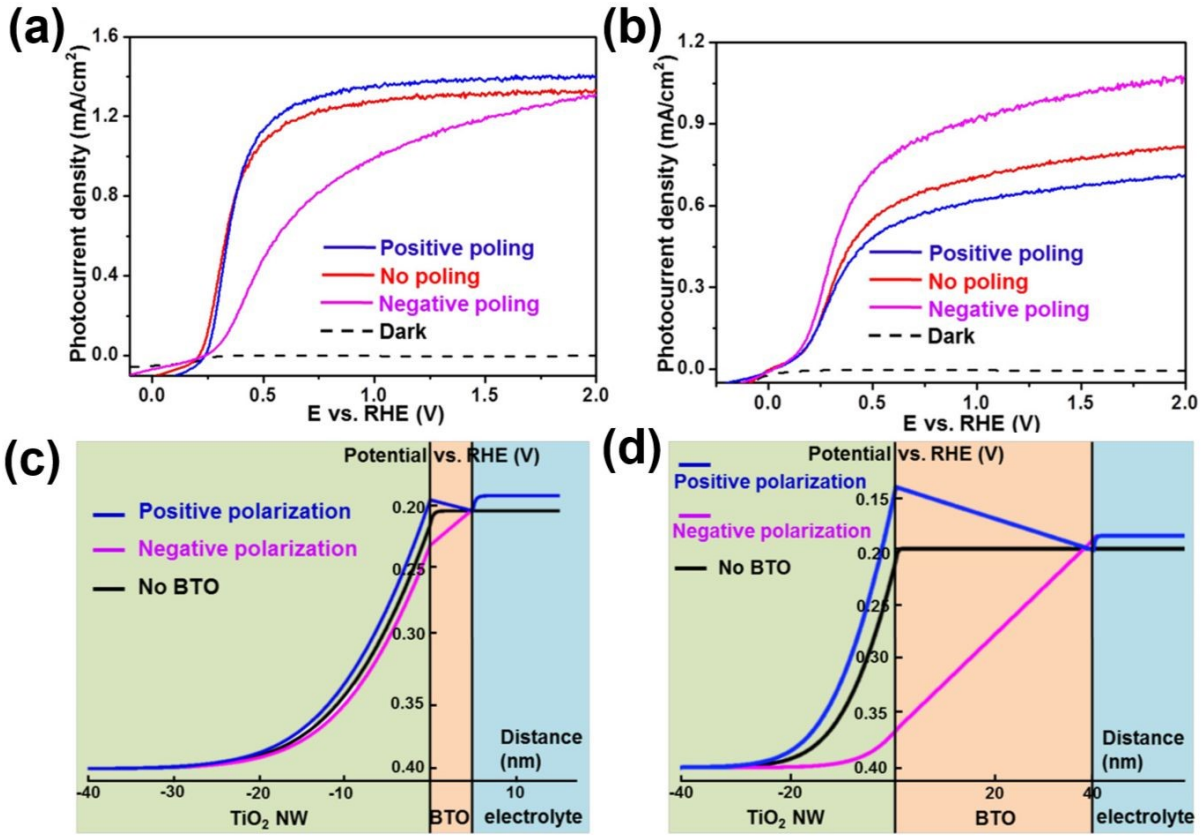

Figure 7. LSV curves of the unpoled (red), positively poled (blue) and negatively poled (magenta) TiO_2/BTO NWs with a BTO thickness of **(a)** 5 nm and **(b)** 40 nm. (c) Calculated potential distribution and electric poling effects on the ferroelectric enhancement in TiO_2/BTO/NaOH heterojunctions with BTO thickness of **(c)** 5 nm and **(d)** 40 nm. Reproduced with permission.[72] Copyright © 2015, American Chemical Society.

In a similar system utilizing TiO_2 nanowires, Wu et al. demonstrated that using STO instead of BTO with interface stress-induced lattice strain in the STO can significantly enhance the

separation and transfer of photogenerated charges.[113] Although ferroelectricity in STO remains controversial, the strained STO was reported to possess ferroelectric properties. To modify the thickness of the STO shell in the TiO_2/STO core/shell NWs, the hydrothermal reaction time was varied. Among the various thicknesses, TiO_2 NWs with a 10 nm-thick STO shell exhibited the highest photocurrent density of 1.43 mA cm^{-2} at 1.23 V_{RHE} (**Fig. 8a**). This represents an impressive improvement (83%) compared to pristine TiO_2 (0.78 mA cm^{-2} at 1.23 V_{RHE}) under the test condition of 1 M NaOH electrolyte and AM 1.5 G illumination. The enhanced performance was attributed to improved charge separation efficiency. The experiments yielded a separation efficiency of 87.7% at 1.23 V_{RHE}, which was 79.3% higher than that observed for pristine TiO_2 NWs. Enhanced performance compared with TiO_2/BTO core/shell NWs was attributed to the better electrical conductivity of STO than BTO (**Fig. 8a**). Like the BTO system, the PEC performance of the TiO_2/STO heterostructure was further enhanced by polarization. Numerical band structure calculations unveiled that, under positive polarization, a negative ferroelectric charge accumulated at the TiO_2/STO interface (**Fig 8b**). The effect amplified band bending in the TiO_2 compared to the unpoled sample resulting enhanced charge separation to slightly boost photocurrent density, with the limited effect attributed to the spontaneous polarization of the STO being predominantly positive. Conversely, negative poling reduced the depletion width of TiO_2 resulting in substantially decreased photocurrent density (**Fig. 8a**). The magnitude and width of the depletion layer are decisive factors in ensuring efficient charge separation.

View Article Online
DOI: 10.1039/D4TA07812H

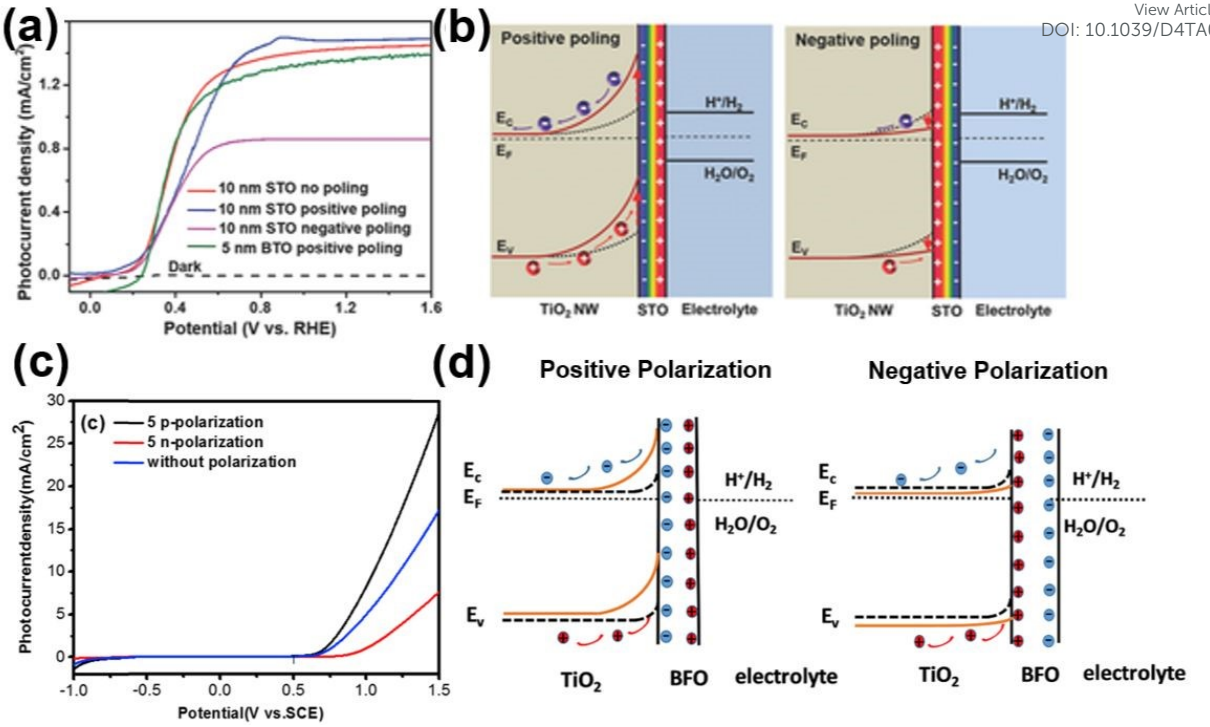

Figure 8. (a) Linear sweep voltammetry (LSV) curves of as-prepared (red), positively poled (blue), and negatively poled (purple) TiO_2/10 nm-STO, as well as positively poled TiO_2/5 nm-BTO (green). **(b)** Schematic depicting the electronic band diagram of the TiO_2/STO interface with positive poling and negative poling conditions. Reproduced with permission.[113] Copyright © 2017, John Wiley and Sons. **(c)** LSV curves under AM1.5G illumination, and **(d)** schematic energy band diagram of positively and negatively poled BFO-5/TiO_2. Reproduced with permission.[114] Copyright © 2019, Elsevier**.**

Beyond BTO and STO, the combination of TiO_2 with BFO has also been explored.[114] A BFO/TiO_2 thin film photoanode with a 50 nm BFO layer exhibited a maximum photocurrent density of 11.25 mA cm^{-2} at 1.5 V_{SCE} in 1 M NaOH under 300 W Xe lamp illumination with AM1.5G filter (**Fig. 8c**). The heterostructure substantially outperformed pristine TiO_2, which produced only 0.33 mA cm^{-2} at 1.5 V_{SCE} under the same conditions. Moreover, the study demonstrated that up-poling the BFO/TiO_2 further enhanced the PEC performance, boosting

the photocurrent density to 28.75 mA cm^{-2} at 1.5 V_{SCE} under identical testing conditions. As schematically shown in **Fig. 8d**, the improvement was attributed to the narrowed space charge region at the BFO/TiO_2 interface for the positively-poled photoanode. This caused an enlarged built-in electric field and upward band bending at the BFO/TiO_2 interface, which resulted in more efficient charge carrier separation. On the contrary, negative polarization reduced the intensity of the band bending, which slowed the carrier separation and thus decreased the current density.

Another commonly used photoactive material in ferroelectric-based composite photoelectrodes is $BiVO_4$ (BVO). The narrow BVO bandgap (2.4 eV) allows it to absorb the visible-light range of the solar spectrum.[93] However, its PEC performance is still low due to unavoidable charge recombination throughout the bulk and at the surface of BVO. Combining BVO with ferroelectric materials can enhance the electron transport properties.[93] This concept was demonstrated by Xie and co-workers, who used a sol-gel method to deposit BFO on BVO and then subjected it to heat treatment at 500°C for 30 min.[21] The resulting BVO/BFO heterostructures produced substantially increased the photocurrent density, 440% higher (0.6 mA cm^{-2} at 1.23 V_{RHE}) with a ~400 mV onset potential shift compared to bare BVO (0.14 mA cm^{-2} at 1.23 V_{RHE}), measured in 0.5 M Na_2SO_4 under AM 1.5 G illumination. The exploitation of ferroelectric polarization in BVO/BFO heterostructures was achieved by applying ± 20 V electrical potential in air. Positive polarization enhanced the BVO/BFO photoanode photocurrent density by 19% compared to the unpoled case. As shown in the inset of **Fig. 9a**, this improvement was attributed to stronger upward band bending at the BFO/BVO interface, which lead to an increased width of the depletion layer (L_D) in BVO. The change in the interfacial energy levels facilitates charge separation and thus leads to the improved PEC performance. In contrast, the opposite effect was observed with negative polarization which induces decreased band bending and narrowed L_D. The photocurrent

View Article Online
DOI: 10.1039/D4TA07812H

density of down-poled BVO/BFO was reported to decrease to 75.6% that of the unpoled sample.

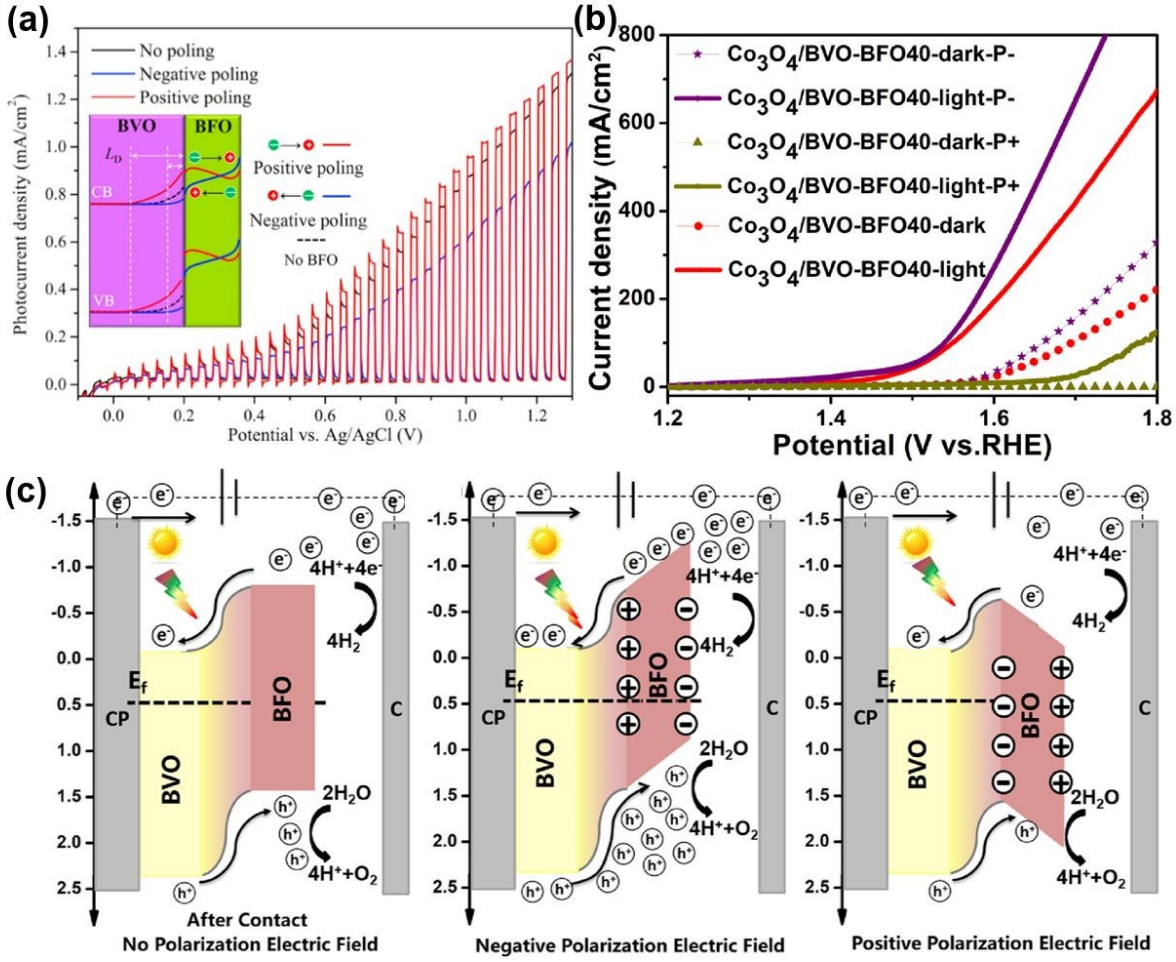

Figure 9. (a) LSV curves of the as-prepared (black), positively poled (red) and negatively poled (blue) BVO/BFO photoanode under 100 mW cm^{-2} visible light. Inset is the schematic mechanism of the charge dynamics tuned by the direction of the polarization (L_D: width of the depletion layer). Reproduced with permission.[21] Copyright © 2017, Elsevier. **(b)** LSV plots for Co_3O_4/BVO-BFO light-off, light-on and ferroelectric-light on and **(c)** energy diagram and possible photogenerated charge pathways in illumination condition under different electric field ferroelectric polarization. Reproduced with permission.[38] Copyright © 2022, Elsevier.

Distinct from the BVO/BFO system prepared by Xie et al., Yang et al. prepared BVO/BFO heterostructures with Co_3O_4 cocatalyst by spin-coating mixed solutions containing bismuth, iron and vanadium precursors.[38] The films did not exhibit distinguishable layers of BVO and BFO, although TEM images indicated heterojunction formation between the BFO and BVO. The as-prepared sample exhibited a photocurrent density of 2.24 mA cm^{-2} at 1.23 V_{RHE}, which was approximately double that of Co_3O_4/BVO. Interestingly, this work demonstrated enhanced PEC performance by polarizing with a negative potential (-30 V DC power for 10 minutes in 1 M KOH solution), realizing an increased photocurrent density of 4.51 mA cm^{-2} at 1.23 V_{RHE}. As shown in **Fig. 9b**, this effect of negative polarization was observed up to 1.8 V_{RHE}. On the other hand, the performance was significantly decreased to 1.23 mA cm^{-2} at 1.23 V_{RHE} with positive polarization. The improvement in negatively poled BVO/BFO was attributed to the modulation of band gradients in BFO as a result of ferroelectric polarization (**Fig. 9c**). Negative polarization results in a positive band gradient in BFO (sloping up towards the SEI), which facilitates hole transfer to the electrolyte. Meanwhile, positive polarization induces a negative band gradient in BFO which leads to accumulation of charge carriers at the BFO/BVO interface, thus invoking higher charge recombination.

It is interesting that these two previous studies reported opposite effects on PEC performance with polarization direction of BFO. While Xie attributed the improved performance of positively poled BFO/BVO to enhanced charge dynamics at the BFO/BVO interface, Yang considered the effect of band gradient in negatively poled BFO/BVO to dominate, thus resulting in better performance compared to positively poled BFO/BVO. In our recent study, we have revealed the interplay between ferroelectric polarization and charge transfer dynamics at the heterojunction interface of a BFO/BVO system.[115] We found that there are two co-existing effects induced by ferroelectric polarization, with the dominant one regulating the overall performance. By having a balance of both effects, we realized

View Article Online
DOI: 10.1039/D4TA07812H

enhanced PEC performance in both polarization directions. The down polarization of BFO/BVO shifts the BFO band energies to lower energy levels, invoking intensified band bending at the SEI and a positive band gradient, delivering a 136% enhancement in photocurrent density compared with the unpoled sample. The negatively shifted electronic states in the down-poled BFO reduced the band offsets at the BFO/BVO heterointerface, reducing the energy barrier for photogenerated charge transfer across the BFO/BVO interface. However, the reduced band offsets also diminish the driving force for charge transfer across the interface and the extent of band bending in BVO near the interface, exposing a tradeoff between the effects of polarization on the heterointerface vs. within the bulk ferroelectric and at the SEI in poled BFO/BVO. The tradeoff is reversed for upward polarized BFO/BVO, where the larger band offset at the heterointerface facilitates band bending and charge separation at the BFO/BVO interface, resulting in increased charge separation efficiency. However, the band gradients in the up-poled BFO layer will impair hole transport to the SEI, resulting in higher resistance for charge transfer to the electrolyte. Nevertheless, in the up-poled BFO/BVO system, the enhanced bulk charge transfer overshadows the other negative effects, therefore a 70% enhancement in photocurrent density (relative to unpoled) at 1.23 V vs. RHE was observed.

Other metal oxides semiconductors such as tungsten oxide (WO_3) and hematite (Fe_2O_3) are also frequently combined with ferroelectric materials for PEC applications.[116-119] For instance, Sima and co-workers fabricated ferroelectric α-Fe_2O_3/BTO photoanodes by hydrothermal synthesis, spin coating, and thermal treatment.[45] The nanowires were approximately 1 μm in length with a BTO layer up to 18 nm thick. Subjecting the nanowires to ferroelectric positive polarization in propylene carbonate offered a 40.4% increase in photocurrent density compared to the equivalent unpoled sample, while negative polarization decreased the photocurrent.

Apart from metal oxides, integrating metal sulfides[55,120,121] or nitride materials[19,122,123] with ferroelectrics like BFO, BTO, $SrZrO_3$ and $Pb(Zr_{0.2}Ti_{0.8})O_3$ (PZT) is a common approach to enhance electron-hole separation in photoanodes with strong visible-light absorption. The previously discussed attributes of BTO complement the advantageous characteristics of CdS, leading to improved performance by BTO/CdS heterojunction photoelectrodes. Fang et al. demonstrated a type-II heterojunction by creating a BTO/CdS heterostructure, which exhibited a photocurrent density of ~0.5 mA cm^{-2} at 0 $V_{Ag/AgCl}$ during sulfite oxidation, ~12 times greater than the neat BTO photoanode due to the internal electric field effect at the BTO/CdS interface.[120] Wang and co-workers, who integrated BFO with a C_3N_4 photocathode, delivered a 2.4 times enhancement in photocurrent density compared to pristine BFO.[19] The improved PEC performance was attributed a type-II heterojunction being formed between BFO and g-C_3N_4, enhancing photogenerated charge carrier separation. Upon positive polarization of the BFO/g-C_3N_4 photocathode, the PEC performance was boosted, with a shift in the onset potential to 0.182 $V_{Ag/AgCl}$ for water splitting in a 0.1 M Na_2SO_4 solution under 100 mW cm^{-2} Xe lamp illumination.

While it has been widely demonstrated that ferroelectric polarization can enhance PEC performance of composite photoelectrodes by accelerating the charge transfer at the interface, there is no single pattern in the polarization direction reported to give improvement; the reported studies variously show improvement in upward, downward, or even both polarization directions depending on the specific case. Nevertheless, here we summarize the general pattern that can provide general guidance for designing ferroelectric composites:

(i) In the case of the ferroelectric material being employed as a photocathode (photoanode), sandwiched between a conductive substrate and another photo-absorber, the positive / upward (negative / downward) polarization would

generally be beneficial as it will facilitate charge transfer to the conductive substrate and/or the other semiconductor.

(ii) In the case of a ferroelectric material deposited on top of a photoabsorber, there will be two interfaces (i.e., heterojunction interface, and SEI) at which the ferroelectric polarization will induce two co-existing, and often competing, effects. The polarization direction that intensifies band-bending at the SEI usually brings about a negative impact to the band-bending at the heterojunction, and *vice versa*. The observed improvement in the PEC performance is thus usually a tradeoff between these effects.

It is worth noting that there might also be effects from formation of and changes in band gradients across the ferroelectric layer, and also changes in the surface adsorption-desorption capabilities that might contribute to the observed polarization effects.

3.3. Chemical Modification

3.3.1. Defect Engineering

In a typical metal oxide ferroelectric-based semiconductor, two types of vacancies may exist: anion vacancies (i.e., oxygen vacancies/O_v) and cation vacancies.[124] Of these, the vacancy type with the lowest energy of formation predominates and, in turn, controls the semiconductor properties. It has been reported that O_v located at the surface of a photoelectrode can serve as active sites where reactions occur.[125,126] Similar to other metal oxides, O_v have also been reported to introduce an impurity band within the bandgap of ferroelectric semiconductors.[127-129] Thus, O_v presence can increase the carrier concentration, enhancing charge transfer and suppressing bulk recombination. Specifically for ferroelectrics, vacancies can undergo electro-migration under the influence of the internal electric field,

leading to a restructured energy barrier at the ferroelectric interface.[8,128,130] Yu et al. conducted a study on Bi_3TiNbO_9 (BNT) nanosheets and discovered a unique synergistic effect between oxygen vacancies and ferroelectric polarization.[131] When BNT nanosheets containing oxygen vacancies (BNT-OV2) were polarized (referred as BNT-OVP), they exhibited a significantly higher remnant polarization and coercive field than the neat BNT (**Fig. 10a**), due to the introduction of O_v impeding displacement of the ions and therefore increasing the energy required to allow the displaced ions to return to their original positions. Consequently, the polarized state persisted for a longer period compared to the BNT sample without O_v. The photocurrent response by BNT, BNT-P (polarized neat BNT), BNT-OV2 and BNT-OVP (**Fig. 10b**) revealed that the presence of oxygen vacancies facilitated absorption of a wider light spectrum (up to 500 nm, compared to 420 nm for neat BNT) due to an intermediate band induced by the oxygen vacancies. However, an excessive O_v presence in ferroelectric materials can adversely impact the ferroelectric properties due to increased electrical conductivity and thus current leakage.[79]

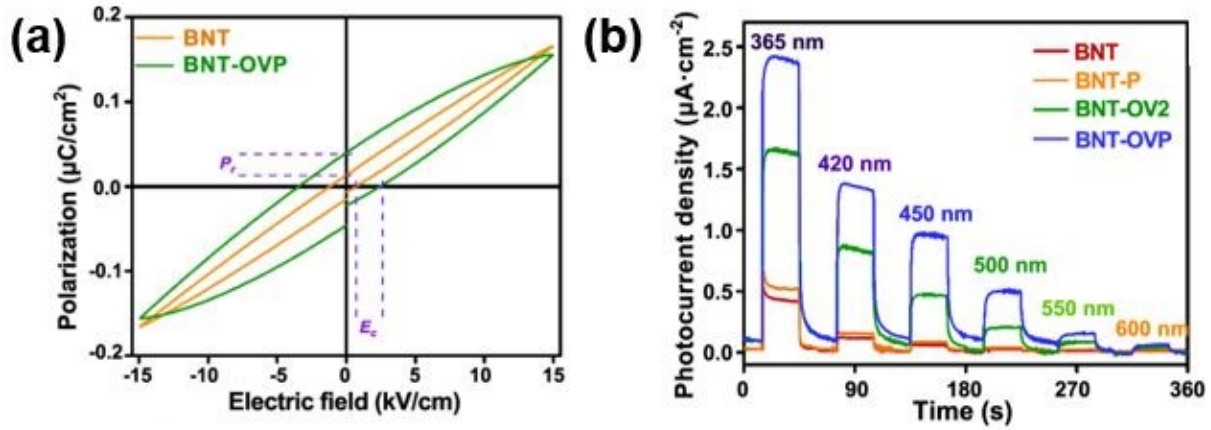

Figure 10. (a) Hysteresis loops for BNT photoanodes with (BNT-OVP) and without (BNT) oxygen vacancies, and **(b)** photocurrent response by BNT, polarized BNT (BNT-P), oxygen vacancy-rich BNT (BNT-OV2) and polarized oxygen vacancy-rich BNT (BNT-OVP) under

light with different wavelengths. Reproduced under terms of the CC-BY license.[131] Copyright © 2018, The Authors, published by Springer Nature.

The presence of oxygen vacancies in metal oxide ferroelectric materials can naturally occur during the synthesis process with their concentration dependent on, for example, the partial oxygen pressure during annealing.[126,132] Xu et al. demonstrated that annealing BFO in oxygen-poor conditions resulted in a higher oxygen vacancy concentration within the material.[133] On this basis, synthesizing oxide materials under a low oxygen atmosphere or vacuum conditions could promote oxygen vacancy formation.[134] In a study by Radmilovic et al., oxygen vacancies were intentionally introduced through heat treatment of BFO thin films under a nitrogen environment, resulting in n-type BFO suitable for use as a photoanode.[135] The flat band potential was reported to shift slightly in the negative direction compared to the defect-free BFO, accompanied by an improvement in photocurrent by 76%. The introduction of oxygen vacancies can also lead to other physical changes in the material, including a change in color.[18,28] Wang et al. demonstrated the effectiveness of high-pressure hydrogenation to introduce oxygen vacancies into BFO. Compared to pristine BFO, the hydrogenated BFO demonstrated an enhanced capability to absorb visible light, accompanied by a decrease in the bandgap of the hydrogenated material.[28]

Other than applying additional treatment on the material, the concentration of oxygen vacancies can be controlled, for example, through varying the ratio of metal ions in sol-gel precursors. Yang et al.[128] conducted a study investigating the impact of oxygen vacancy concentration on BFO performance by varying the bismuth content in the precursor solution. They demonstrated that precursor solutions with a lower bismuth content produced films with poorer morphology and a higher concentration of oxygen vacancies. Prasad and co-

workers[136] reported 100% enhancement in the photocurrent density (measured at 0.6 V vs. RHE) of a BFO photocathode synthesized with 10% excess bismuth in the precursor solution compared to the stoichiometric counterpart. This improvement was attributed to a lower recombination rate and lower charge transfer resistance in the 10% excess bismuth BFO, due to the presence of fewer vacancies which can act as recombination centers.

While anion vacancies are the most common form of defects, recent reports have highlighted the potential benefits of metal cation vacancies in ferroelectric-based photoelectrodes.[137,138] Cation vacancies have been demonstrated to play similar roles to anion vacancies in modifying the catalytic properties of nanomaterials.[139] They can reduce activation energies for surface reactions by altering the reaction mechanism at the photoelectrode active sites. Further, cation vacancies have been found to impact the ferroelectricity of materials. For example, the formation of strontium (Sr) vacancies in STO can give rise to room-temperature ferroelectricity, when STO is otherwise paraelectric,[137,138] opening up an avenue to enhance the PEC performance of STO-based photoelectrode systems. It is worth noting that there are a substantial number of studies available on materials rich in anion vacancies, while there are relatively few reports on ferroelectric-based photoelectrodes with an abundance of metal cation vacancies. The high formation energy of metal cation vacancies may be a barrier in this regard. Greater effort is needed in this emerging research area to advance the development of cation vacancy-rich photoelectrodes. Many studies have demonstrated the benefits of vacancies within ferroelectric photoelectrodes; however, some works have also pointed out problems associated with the presence vacancies. Therefore, finding the delicate balance is required when controlling the vacancies within a material to optimize its properties and functionality.

View Article Online
DOI: 10.1039/D4TA07812H

3.3.2. Doping

To address the issue of limited light absorption due to the wide bandgap of perovskite oxide ferroelectrics, doping can be employed to enhance light harvesting.[9,140] When metal ions are introduced into a ferroelectric crystal lattice through doping, they usually create a narrow energy band within the bandgap. This, in turn, makes it easier to produce photoexcited electrons and extends the photo-responsive wavelength into the visible region. For instance, a study by Hu et al. demonstrated that the bandgap of a PTO photocathode could be reduced from 3.4 eV to 3.2 eV by doping it with iron.[66] The bandgap reduction derived from the formation of energy levels around 0.2 eV below the PTO conduction band. With doping, the photocurrent of the PTO photocathode significantly increased from 38 μA cm^{-2} to 120 μA cm^{-2} at 0 V_{SCE} in 0.1 M Na_2SO_4 under 100 mW cm^{-2} Xe lamp illumination.

The PEC performance of an Ag/Nb-doped ferroelectric STO photoanode in unpoled and poled conditions was examined by Singh et al.[141] The unpoled photoanode yielded a photocurrent density of 93 μA cm^{-2} at 1 $V_{Ag/AgCl}$, with an onset potential at −0.74 $V_{Ag/AgCl}$. The positively poled sample demonstrated an enhanced photocurrent density of 130 μA cm^{-2} at 1 $V_{Ag/AgCl}$, accompanied by a 20 mV reduction in the onset potential. However, under the same test conditions, negatively poled samples displayed a reduced photocurrent density of 40 μA cm^{-2} at 1 $V_{Ag/AgCl}$ with a positive shift in the onset potential by 20 mV. The trends in photocurrent are seen through the amperometry test results (**Fig. 11a**). Ag/Nb doping introduced sufficient free charge carriers in the STO to flatten the electronic bands. A negative shift in the flat-band potential for the sample with positive polarization compared to the negatively poled sample was observed through a Mott-Schottky test (**Fig. 11b,c**). As schematically shown in **Fig. 11d**, at the STO-electrolyte interface, the energy bands were bent upwards, creating a space charge region (W_{sc}). Positive polarization enlarged the W_{sc}

View Article Online
DOI: 10.1039/D4TA07812H

width at the STO-electrolyte interface, enhancing the potential gradient and driving more holes towards the interface to facilitate charge transfer to the electrolyte. The extended W_{sc} also provided a larger region within the STO for effective separation of photogenerated electron–hole pairs by the built-in potential. In contrast, negative polarization had the opposite effect on the interfacial band structure. The W_{sc} was reduced which lowered the interfacial charge density, hindered electron–hole separation and diminished PEC performance.

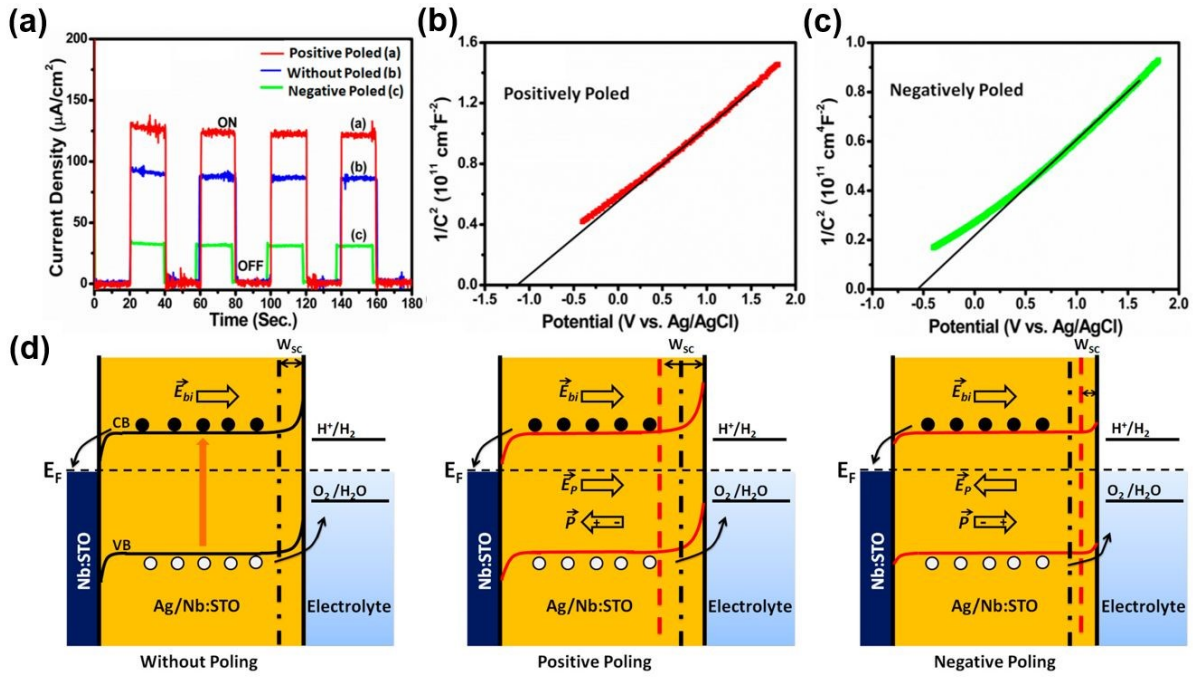

Figure 11. (a) Chronoamperometry test at 0.5 V vs. Ag/AgCl, and Mott–Schottky plots of (b) positively and (c) negatively poled Ag/Nb:STO photoelectrodes. (d) Schematic illustration of the electronic band structure of ferroelectric Ag/Nb:STO under different polarization conditions. E_{bi}: intrinsic built-in electric field; E_p: induced polarization electric field; W_{sc}: space charge region width; P: polarization; CB: conduction band; VB: valence band. Reproduced with permission.[141] Copyright © 2019, American Chemical Society.

View Article Online
DOI: 10.1039/D4TA07812H

View Article Online
DOI: 10.1039/D4TA07812H

6. Experimental Aspects

Beyond photoelectrode materials selection and design, it is important to consider experimental aspects such as fabrication method, poling technique and electrolyte selection. These experimental factors which require consideration during the design and testing of ferroelectric photoelectrodes are examined in the ensuing sections.

6.1. Fabrication Method

As summarized in **Table 1**, one of the methods commonly used to synthesize ferroelectric photoelectrodes is the hydrothermal method. Hydrothermal is a process of crystallizing a substance at high temperature (i.e., higher than the boiling point of solvent) and high pressure in an aqueous solution. The hydrothermal process offers control over the morphology and size of the fabricated ferroelectric nanostructures by tuning the temperature, reaction time, pH of the solvent, and also the concentration of the metal precursors.[142] The hydrothermal method has been demonstrated to fabricate $BaTiO_3$[13,45,72], $BiFeO_3$[119], $NaNbO_3$[35,81], doped-ZnO[143], doped-STO[144] photoelectrodes. For example, Yang et al. controlled the thickness of the ferroelectric $BaTiO_3$ layer on TiO_2 nanowire photoanodes by varying the hydrothermal reaction temperature.[72] The thickness of the $BaTiO_3$ on TiO_2 was observed to increase from 5 nm to 40 nm when the temperature was increased from 150 to 210 °C due to an accelerated $BaTiO_3$ synthesis rate.

Apart from hydrothermal, sol-gel is another adopted method due to its simplicity. Sol-gel synthesis generally starts by the deposition of a precursor solution onto a substrate – normally through a dip-coating or spin-coating process, followed by a subsequent gelation (drying) process at low temperature (<100 °C) prior to a high-temperature crystallization step.[145] The concentration of metal precursors, chelating agent, solvent, coating speed (i.e., spinning rate for spin-coating or withdrawing speed for dip-coating), viscosity, gelation temperature,

View Article Online
DOI: 10.1039/D4TA07812H

crystallization temperature, and annealing atmosphere all play pivotal roles in determining the morphology, crystal size, phase, and thickness of the photoelectrode synthesized. For example, work by Zhang and co-workers demonstrated that the quality of sol-gel-derived $BiFeO_3$ is highly influenced by the metal nitrate concentration in the precursor solution.[90] Increasing the metal nitrate concentration will induce precipitation during the drying process due to the accelerated drying rate of the organic solvent. The precipitates will lead to the formation of secondary phases (i.e., impurities) in the $BiFeO_3$ films.

Despite their advantages, the hydrothermal and sol-gel processes most of the time result in polycrystalline material, in which, for ferroelectric materials, the non-aligned domains may reduce the magnitude of ferroelectric polarization.[89] A study on lead lanthanum zirconate titanate (PLZT) films with a Au/PLZT/Pt structure underscores the importance of having a single growth oriented crystal within the thin films, with a uniform polarization direction producing a significantly larger photocurrent compared to a randomly-oriented polycrystalline PLZT film.[146] Nevertheless, in order to get single-crystal ferroelectric photoelectrodes, there are two main requirements: (i) high precision fabrication techniques, and (ii) suitable substrate that promotes crystal growth in specific orientation. Highly precise fabrication methods, such as sputtering oxide molecular beam epitaxy (OMBE),[147] physical vapor deposition (PVD),[148] or chemical vapor deposition (CVD),[149] have dominated the scene for realization of high quality ferroelectric thin films. However, their scalability is a significant commercial challenge. For instance, the popular method for epitaxial growth of pulsed laser deposition (PLD) can typically only synthesize samples with a size of several square millimeters, and thus is not feasible for large-scale production.

The second important aspect is the substrate selection, as single-crystal growth usually requires a substrate that induces growth of crystals with a specific orientation (e.g., $SrTiO_3$, $LaAlO_3$, MgO). Interestingly, with a proper substrate selection, a single crystal ferroelectric

View Article Online
DOI: 10.1039/D4TA07812H

thin film can be grown with simpler methods, such as sol-gel, if precise control of synthesis parameters is realized. For example, Zhang et al. fabricated a 150 nm-thick (001)-oriented $BiFeO_3$ epitaxial thin film on a lanthanum strontium manganese oxide (LSMO)/STO (001) substrate with sol-gel method.[90] The as-synthesized thin film exhibited ferroelectric properties that are comparable with PLD-derived $BiFeO_3$ (001)-oriented epitaxial thin films. However, this approach also presents economic challenges for scaling up as such substrates are expensive. Interesting studies in solar cell technology have reported that pre-treatment of the conductive substrates that are often used in PEC systems (i.e., FTO and ITO) can promote a preferred growth orientation.[150,151] Given the promises of this technique in dictating the crystal growth orientation, there is a vast opportunity to adopt pre-treatment of substrates to promote preferred growth orientation of ferroelectric photoelectrodes.

6.2. Poling Method

Domain switching or polarization is defined as the process of aligning the domains in a ferroelectric material in a specific direction. It is usually achieved by imposing a strong electric field on the ferroelectric material.[152-154] The process involving application of a strong electric field may induce structural changes in the photoelectrode, thus careful selection of the poling method has to be considered, as it can significantly affect the ferroelectric properties and PEC performance.

One common method to pole a ferroelectric material is by DC poling.[155-157] During DC poling, the ferroelectric sample is sandwiched between a top and a bottom metal electrode (**Fig. 12a**). DC Poling is commonly conducted in an isolated environment, such as a mineral oil or an inert atmosphere, to insulate the material from excessive electric discharge.[158] The poling commences by gradually increasing the DC voltage until the desired electric field (5-

View Article Online
DOI: 10.1039/D4TA07812H

1000 kV cm^{-1}) is attained, based on a saturation polarization value. This poling method possesses several drawbacks, such as the need for a conductive coating (e.g., silver paste) to be applied to the photoelectrode surface (i.e., the silver paste acts as top electrode during the DC poling). Unless properly removed, this coating will impose extraneous effects on any subsequent PEC performance test. Removing the coating requires contact with a solvent and/or application of force (e.g., sonication or scrubbing) which may de-pole the sample.

Unlike DC poling, corona poling requires metallization on a single side of the ferroelectric sample only and is more practical for ferroelectric photoelectrode fabrication. During corona poling (**Fig. 12b**), a high voltage (8 – 20 kV) is applied to a needle , causing break-down of the gas molecules near the needle tip to produce a corona discharge.[152,155,159-161] Exposure of the ferroelectric sample to this corona discharge causes poling. A metallic grid, held at a lower voltage (0.2 – 3 kV), is placed between the needle and the ferroelectric sample to distribute the ionized charges across the sample, giving better uniformity of poling. The number of charges reaching the ferroelectric sample surface is controlled by the grid location and the applied voltage.

Polarization of a ferroelectric photoelectrode can also be accomplished by electrochemical poling (**Fig. 12c**). In this method, a two-electrode set up (counter electrode and working electrode) is usually used, even though some studies demonstrate the use of a three-electrode configuration (counter electrode, working electrode and reference electrode). In electrochemical poling, propylene carbonate is usually used as the electrolyte solvent owing to its large electrochemical window that eliminates the possibility of electrolyte reduction or oxidation during the poling process.[20,45,162] Lithium perchlorate is usually used as the electrolyte in the organic solvent system as it has good solubility in the organic medium. Alternatively, some researchers have demonstrated that polarization can be done in aqueous media with NaOH[163], KCl[17,72] or KOH[38] as the electrolyte (Table 1).

View Article Online
DOI: 10.1039/D4TA07812H

Even though many studies have demonstrated effective poling methods for ferroelectric photoelectrodes, there is still a lack of systematic studies on the effects of different polarization methods on the PEC performance of photoelectrodes. In the corona poling method, the ferroelectric surface is less affected by chemical changes, as it is only in contact with a gaseous environment. However, in the electrochemical method, the surface of the ferroelectric thin film may interact with the water/solvent used, leading to hydration or other changes in surface chemistry. The XPS and DFT results in our previous work show that the BFO surface termination is strongly influenced by the interaction between the polarized surface and water.[115] Consequently, our work (electrochemical poling) likely resulted in a different terminating layer and hence differences in the observed PEC performance compared to Xie et al.[21] (poling in air), as discussed earlier (Section 3.2.2). It should be noted that there may also be effects associated with provenance of samples and details of PEC measurement contributing to the differences in results.

Careful consideration of parameter suitability (e.g., temperature, mechanical stress, sample geometry, and chemical compatibility) is required when choosing the poling method, and in addition to choosing an appropriate poling method, such poling parameters must also be considered and tuned to effectively pole the material and optimize the PEC performance. Different poling methods require tuning of different parameters such as voltage, temperature, poling duration and inert gas used. The degree of alignment of the dipoles in a ferroelectric material depends on both intrinsic and external factors such as the uniformity and duration of the applied electric field, and factors related to the sample being poled, including its size, manufacturing procedure, and the presence and concentration of defects, impurities, pores, and dopants.[59,64,131,164-166] During the poling process, the application of mechanical stress can affect the domain-wall movement.[86,167-169] Among all the influential factors, the strength of the applied electrical field, and poling temperature and duration, are generally the most

View Article Online
DOI: 10.1039/D4TA07812H

critical parameters affecting the poling of ferroelectric materials and the consequent PEC performance.

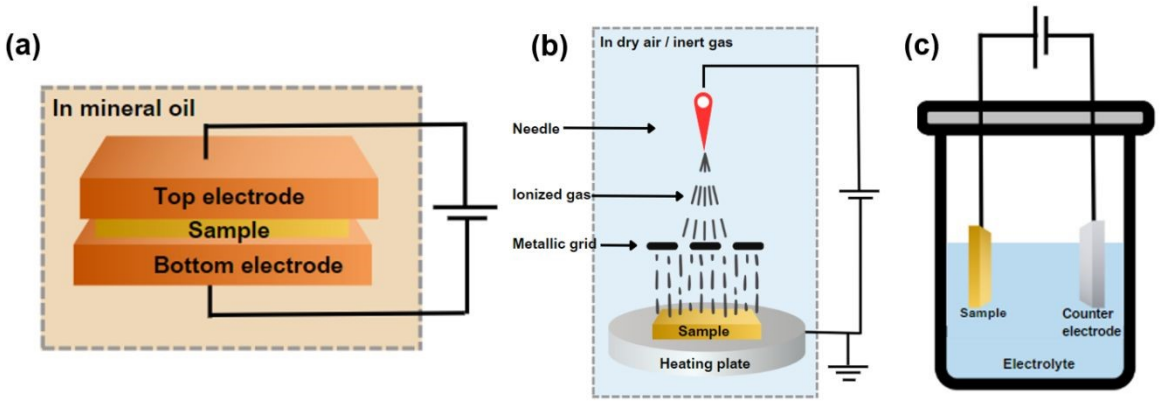

Figure 12. Schematic depicting various poling systems; **(a)** DC poling, **(b)** corona poling, and **(c)** electrochemical poling.

Apart from the above, there is also a challenge in developing in-situ poling methods. With current poling methods, in order to switch the polarization state, the photoelectrode needs to be taken out from the PEC reaction system, poled, and then put back into the reaction system, which is not practical in terms of allowing dynamic polarization switching. To harness the full potential of a ferroelectric photoelectrode, i.e., to achieve control of reaction activity and selectivity by tailoring the adsorption/desorption strength of all reactants, intermediates and products, it must be possible to dynamically control the polarization state over the course of the reaction to allow surface chemistry to be independently optimized for each reaction step. This requires an in-situ polarization method. However, a simple yet effective, and rapid, in-situ poling method remains elusive, which opens a vast opportunity for the community to develop such methods to allow agile and dynamic ferroelectric photoelectrodes and fully exploit their potential in PEC applications.

View Article Online
DOI: 10.1039/D4TA07812H

6.3. Electrolyte Selection

Electrolyte solution plays a vital role in photoelectrocatalysis in general, especially in determining the charge transfer behavior at the semiconductor-electrolyte interface. Despite the importance of electrolyte selection, no studies are available which specifically investigate the effect of electrolyte on PEC performance for ferroelectric materials. Tian et al. demonstrated that exposing epitaxial BFO to solutions with different pH could drive reversible bulk polarization switching.[170] The OH^- and H^+ ionic adsorption and interaction on the BFO surface provide a driving force to induce upward or downward bulk polarization, respectively. This phenomenon was analyzed by phase-field simulations which suggested that negative charge accumulation from OH^- ions on the BFO surface can lead to polarization reversal from a downward to an upward state. Conversely, the positive charge from H^+ could instigate polarization reversal from an upward to a downward state as shown in **Fig. 13a-d**. It was reported that contact with acetone did not affect the polarization states. Thus, identifying the correct pH conditions is critical to retain the desired polarization direction of ferroelectric photoelectrodes during a PEC process. Employing a non-aqueous electrolyte (e.g., acetonitrile) offers an alternative to retain the polarization state of a ferroelectric photoelectrode. However, this approach comes with challenges related to potential environmental impact and the toxicity of organic solvents.

View Article Online
DOI: 10.1039/D4TA07812H

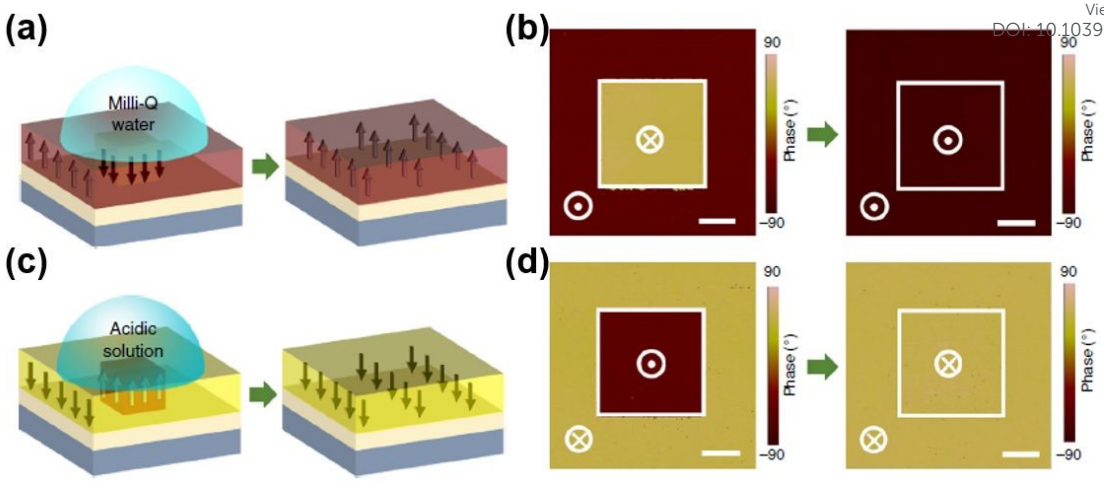

Figure 13. Schematic illustration of BFO switching from downward/upward after exposing the films to **(a)** Milli-Q water (neutral) and **(c)** acidic solution. **(b)** and **(d)** show the corresponding piezoresponse force microscopy (PFM) images (scale bar is 2 μm). Reproduced under terms of the CC-BY license.[170] Copyright © 2018, The Authors, published by Springer Nature.

Careful selection of the electrolyte type (i.e., acidic, neutral, or basic) is also necessary to restrict photoelectrode corrosion during the PEC process. Pourbaix diagrams can provide guidance on electrolyte selection for specific ferroelectric materials. However, reports of detailed Pourbaix diagrams for ferroelectrics are relatively rare in the literature.

7. Outlook and Perspective

Ferroelectric materials hold significant promise as photocathodes or photoanodes in PEC applications due to their polarization-induced internal electric field and switchable surface properties, which can be exploited to improve charge transport and separation, and to gain better control over reaction activity and selectivity. The current review discussed the essential

design criteria and strategies for employing ferroelectrics in PEC systems based on reported experiences, providing valuable insights on the future of ferroelectric photoelectrodes. High-quality photoelectrodes must excel in three key areas: (i) superior light absorption and charge generation; (ii) efficient charge transfer; and (iii) rapid charge consumption. Of these three attributes, ferroelectrics offer particular potential in maximizing charge transfer and charge consumption beyond conventional semiconductors. In order to harness the full potential of ferroelectric materials, exploiting the polarization to optimize aspects (ii) and (iii) while ensuring good light absorption (e.g., through identifying low bandgap ferroelectrics, implementing bandgap modification strategies, or incorporating ferroelectrics in heterostructures) is particularly important. It has also been emphasized throughout the discussion that the thickness of a ferroelectric layer, both in standalone photoelectrode systems and heterostructures, is an influential factor for overall PEC performance and should be carefully considered and controlled.

To advance the ferroelectric-based photoelectrode field, we propose three significant focal points for future development:

1. **Exploring alternative reactions.** Several studies suggest that polarizing a ferroelectric photoelectrode can regulate the adsorption strength at the surface of the photoelectrode. Water splitting, which is the most explored PEC reaction to date, involves sluggish water oxidation at the photoanode surface which restricts efficiency. Replacing the water oxidation reaction with faster reactions for clean fuel production, such as biomass oxidation, that require a lower energy input will enhance overall efficiency.[171,172] However, complex reactions such as biomass oxidation face challenges in product selectivity. Ferroelectric photoelectrodes can offer a unique advantage here, through using the polarization-dependent surface chemistry to provide control over adsorption/desorption and reaction processes and hence products

View Article Online
DOI: 10.1039/D4TA07812H

formed beyond what is possible with conventional semiconductor photoelectrodes that present only a single, static surface chemistry. Combining the lower energy requirements of alternative reactions to water oxidation with the controllable surface properties of ferroelectrics will advance the field of photoelectrochemical clean fuel production.

2. **Optimizing fabrication methods.** Available studies have demonstrated that single crystal ferroelectric photoelectrodes generally result in enhanced performance compared to polycrystalline systems. However, fabricating epitaxial single-crystal thin films requires expensive techniques and/or substrates that promote single-crystal growth. Such fabrication methods are not applicable for energy-harvesting technologies, where large-scale, low-cost devices are required. Therefore, future work needs to address these issues by two approaches: (i) Searching for economical and scalable substrates that promote epitaxial single-crystal growth, and (ii) promoting research on low-cost, scalable and uniform techniques for fabrication of polycrystalline ferroelectric materials with good ferroelectric properties on relatively cheap substrates (e.g., ITO, FTO, carbon-based, nickel foam, iron foam). A promising approach that should be investigated further is applying a pre-treatment to substrates to enable crystal growth in a preferred orientation, since optimizing this method presents a vast opportunity to realize efficient ferroelectric photoelectrodes.
3. **Ferroelectric polarization method and retention.** Polarization has been proven to accelerate charge transfer and enhance overall PEC performance. However, many polarization methods demonstrating substantial improvements in photocurrent density are conducted ex-situ (i.e., outside the reaction medium). Additionally, the improvements in PEC performance induced by polarization are typically short-lived, lasting only a few minutes to hours due to charge relaxation. Thus, it is imperative to

develop fast, in-situ methods for polarizing ferroelectric photoelectrodes within the operating medium to regenerate the polarization or rapidly change the polarization direction. This is particularly important to enable full exploitation of dynamic control over the desired photoelectrode surface and electronic states, to allow independent optimization of each reaction step, e.g. for selectivity control in complex reactions such as biomass oxidation as mentioned above.

Author contributions

M. Gunawan and C.Y. Toe generated the concepts, constructed and outlined the draft of the review paper. M. Gunawan contributed to scientific writing of the manuscript. M. Gunawan constructed figures and tables for illustrations. M. Gunawan, S. Zhou, D. Gunawan, Q. Zhang, J. N. Hart, N. Valanoor, R. Amal, J. Scott and C. Y. Toe contributed to review and editing of the manuscript. All authors contributed to the final polishing of the manuscript.

Acknowledgements

This work was financially supported by Australian Research Council (ARC) through Discovery Project (DP210102694), Training Centre for the Global Hydrogen Economy (IC200100023), Centre of Excellence in Future Low-Energy Electronics Technologies (CE170100039), and Centre of Excellence for Carbon Science and Innovation (CE230100032). Q.Z. acknowledges the support of a Women in FLEET Fellowship

Table 1. A summary of PEC performance of ferroelectric photoelectrodes.

Material	**Synthesis method**	**Photocurrent density** (at 1.23 V_{RHE} and AM1.5 G, unless otherwise specified)	**Electrolyte**	**Poling method**	**Polarization induced enhancement** (at 1.23 V_{RHE}, unless otherwise specified)	**Ref.**
BFO with oxygen vacancies	Electrodeposition	450 μA cm^{-2}	Borate buffer (pH = 9.2) & 0.7 M sulfite	N.A.	N.A.	[135]
14 nm LFO/STON	PLD	0.55 mA cm^{-2} (Laser light, 5 mW, 405 nm)	0.5 M NaOH	N.A.	N.A.	[34]
$BiVO_4/BiFeO_3$	Dip coating and sol-gel	0.28 mA cm^{-2}	0.5 M Na_2SO_4	±20 V in air	0.32 mA cm^{-2}	[21]
$Co_3O_4/BiVO_4$-$BiFeO_3$	Sol-gel	2.24 mA cm^{-2}	1 M KOH	±30 V in 1 M KOH	4.51 mA cm^{-2}	[38]
3%-wt BTO–WO_3	Drop-casting	37.8 μA cm^{-2}	0.5 M PBS	±20 V in air	63 μA cm^{-2}	[173]
3%-wt BTO –TiO_2	Drop-casting	28 μA cm^{-2}	0.5 M PBS	N.A.	N.A.	[173]
3%-wt BTO–$CuWO_4$	Drop-casting	5.8 μA cm^{-2}	0.5 M PBS	N.A.	N.A.	[173]

Ag/Nb:$SrTiO_3$	PLD	98 μA cm^{-2} (A tungsten halogen lamp, ~100 mW cm^{-2})	0.5 M NaOH	±8 V	128 μA cm^{-2}	141
WO_3/$BaTiO_3$	Drop-casting	52 μA cm^{-2} (UV lamp, 10 mW cm^{-2}, 365 nm)	0.5 M PBS	±20 V	92 μA cm^{-2}	174
CdS/$BaTiO_3$	Hydrothermal	160.46 μA cm^{-2}	0.2 M Na_2SO_3 and 0.1 M Na_2S	±3 V in 0.2 M Na_2SO_3 and 0.1 M Na_2S	459.53 μA cm^{-2}	13
TiO_2-$BaTiO_3$ Core-Shell	Hydrothermal	1.30 mA cm^{-2}	PBS	+3 V or -2 V in 2 M KCl, 5 min	1.50 mA cm^{-2}	72
WO_3/$BiVO_4$/$BiFeO_3$	Sol-gel	1.30 mA cm^{-2}	0.5 Na_2SO_4	N.A.	N.A.	116
$BiFeO_3$/Sn:TiO_2	Hydrothermal & Sol-gel	1.47 mA cm^{-2}	1 M NaOH	±2 V in 1 M KOH	1.76 mA cm^{-2}	107
Ag-doped $BiVO_4$/$BiFeO_3$	Spin-coating	0.51 mA cm^{-2}	0.1 M Na_2SO_4 (pH=6.5)	N.A.	N.A.	77
Sm-doped BFO@RGO	Spin-coating	2.40 mA cm^{-2} at 0.5 V_{SCE}	1 M NaOH	N.A.	N.A.	175
TiO_2/BTO/Ag_2O	composite-hydroxide-mediated (CHM)	1.3 mA cm^{-2} (150 W Xe lamp, AM1.5G)	1 M NaOH	±2 V in 1 M NaOH, 60 s	1.55 mA cm^{-2}	163
WO_3/$BiFeO_3$	Sol-gel	300 μA cm^{-2}	0.5 Na_2SO_4	N.A.	N.A.	117

α-Fe_2O_3/$BaTiO_3$	Sol-gel and hydrothermal	235 μA cm^{-2}	1 M NaOH	±8 V in propylene carbonate, 60 s	330 μA cm^{-2}	45
OEC/CTF/BTO	Hydrothermal	0.83 mA cm^{-2}	1 M KOH	N.A.	N.A.	71
BTO/CdS	Hydrothermal and SILAR	0.5 mA cm^{-2} (300 W Xe lamp)	0.25 M Na_2SO_3 and 0.35 M Na_2S	N.A.	N.A.	120
BTO/TiO_2/CdSe QDs	Hydrothermal	~13.8 mA cm^{-2}	0.25 M Na_2S and 0.35 M Na_2SO_3	±10 V in 0.1 M LiClO4 in propylene carbonate, 60 s	15.3 mA cm^{-2}	29
$BaTiO_3$/$NiFe_2O_4$	Hydrothermal	0.34 mA cm^{-2} at 1.6 V_{SCE}	1 M KOH	N.A.	N.A.	112
$PbTiO_3$@TiO_2	Doctor blade casting method	0.30 mA cm^{-2}	0.1 M KOH	N.A.	N.A.	69
PVDF/Cu/PVDF-$NaNbO_3$	Hydrothermal	0.1 mA cm^{-2}	0.5 M NaOH	N.A.	0.15 mA cm^{-2}	81
V doped ZnO	Hydrothermal	1.75 mA cm^{-2}	0.5 Na_2SO_4	+2 V or -1.2 V in 0.5 Na_2SO_4, 20 mins	1.9 mA cm^{-2}	176
$NaNbO_3$	Hydrothermal	0.31 mA cm^{-2} at 1$V_{Ag/AgCl}$	0.5 Na_2SO_4	5 V, contact mode	0.51 mA cm^{-2} at 1 $V_{Ag/AgCl}$	35
Li-doped ZnO	Hydrothermal	0.4 mA cm^{-2}	0.5 Na_2SO_4	100 kV cm^{-1}, contact mode	0.48 mA cm^{-2}	143

Fe_2O_3/PZT	Spin-coating	1.0 mA cm^{-2}	1 M NaOH	±5 V in 1 M KCl	1.25 mA cm^{-2}	177
TiO_2/STO	Hydrothermal	1.4 mA cm^{-2}	1 M NaOH	±10 V, contact mode	1.45 mA cm^{-2}	113
Bi_2FeCrO_6	PLD	0.10 mA cm^{-2}	1 M Na_2SO_4	±15 V, contact mode	0.15 mA cm^{-2}	178
BVO@BTO	Spin-coating	3.9 mA cm^{-2}	PBS and 0.1 M Na_2SO_3	N.A.	N.A.	179
$BaTiO_3$/Nb:$SrTiO_3$	Atomic oxygen assisted molecular beam epitaxy	0.09 mA cm^{-2}	0.1 M NaOH	±8 V in propylene carbonate, 10s	0.21 mA cm^{-2}	54
BTO/Cu_2O	Hydrothermal and electrodeposition	0.26 mA cm^{-2} at 0 $V_{Ag/AgCl}$	0.1 M NaOH	N.A.	N.A.	180
Cr-doped $SrTiO_3$/TiO_2	Hydrothermal	4.05 mA cm^{-2} at 0.6V_{SCE} (Xe lamp, 200 mW cm^{-2}, 420 nm cut-off filter)	1 M NaOH	N.A.	N.A.	144
$BiFeO_3$/Fe_2O_3	Hydrothermal	0.57 mA cm^{-2} at 1.7 V_{RHE}	0.5 M Na_2SO_4	N.A.	N.A.	119
α-Fe_2O_3/$BaTiO_3$	Hydrothermal	235 μA cm^{-2}	1 M NaOH	±8 V in propylene carbonate, 60s	330 μA cm^{-2}	45
(111)-oriented $BiFeO_3$	PLD	-45 μA cm^{-2} (500 W Xe, AM1.5G)	0.5 M Na_2SO_4	N.A.	N.A.	75
$BiFeO_3$/Cu_2O	Sol-gel and RF	-103 μA cm^{-2} at -0.4	0.1 M Na_2SO_4	±8 V in 0.1 M	-200 μA cm^{-2} at -0.4	39

	sputtering	$V_{Ag/AgCl}$ (350 W Xe lamp)		Na_2SO_4	$V_{Ag/AgCl}$	
ITO/nano-Au/PZT	Sol-gel	-0.01 mA cm^{-2} (300 W Xe lamp, 455-nm-low pass)	0.1 M Na_2SO_4	±10 V in 0.1 M $LiClO_4$ in propylene carbonate	N.A.	20
PZT/CdS	Chemical bath deposition	-8 μA cm^{-2}	0.1 M Na_2SO_4	±10 V in 0.1 M $LiClO_4$ in propylene carbonate	-10.6 μA cm^{-2}	56
(101)-oriented PZT	PLD	31μA cm^{-2}	1 M KCl	±5 V in 1M KCl	-30 μA cm^{-2}	17
BFO on $Pt/Ti/SiO_2/Si_{(100)}$	Sol-gel	15 μA cm^{-2} (300 W Xe lamp)	0.1 M Na_2SO_4	±8V in 0.1 M Na_2SO_4	N.A.	104
$CuInP_2S_6$	chemical vapor transport	-11 μA cm^{-2}	0.1 M H_2SO_4	N.A.	N.A.	181

REFERENCES

1 Sendeku, M. G. *et al.* Frontiers in photoelectrochemical catalysis: A focus on valuable product synthesis. *Adv. Mater.* **36**, 2308101 (2024).

2 Faunce, T. *et al.* Artificial photosynthesis as a frontier technology for energy sustainability. *Energy Environ. Sci.* **6**, 1074-1076 (2013).

3 Liu, D. & Kuang, Y. Particle-based photoelectrodes for PEC water splitting: Concepts and perspectives. *Adv. Mater.* **36**, 2311692 (2024).

4 Wu, H. *et al.* Photocatalytic and photoelectrochemical systems: Similarities and differences. *Adv. Mater.* **32**, 1904717 (2020).

5 Shi, X. *et al.* Unassisted photoelectrochemical water splitting beyond 5.7% solar-to-hydrogen conversion efficiency by a wireless monolithic photoanode/dye-sensitised solar cell tandem device. *Nano Energy* **13**, 182-191 (2015).

6 Antón-García, D. *et al.* Photoelectrochemical hybrid cell for unbiased CO_2 reduction coupled to alcohol oxidation. *Nature Synthesis* **1**, 77-86 (2022).

7 Wei, X.-K. *et al.* Progress on emerging ferroelectric materials for energy harvesting, storage and conversion. *Adv. Energy Mater.* **12**, 2201199 (2022).

8 Jan, A. *et al.* In operando optical tracking of oxygen vacancy migration and phase change in few nanometers ferroelectric HZO memories. *Adv. Funct. Mater.* **33**, 2214970 (2023).

9 Ma, M. *et al.* Carrier and oxygen vacancy engineering of aliovalent ion modified $BiFeO_3$ and their gas sensing properties. *Sens. Actuators, B* **370**, 132400 (2022).

10 Rørvik, P. M., Grande, T. & Einarsrud, M.-A. One-dimensional nanostructures of ferroelectric perovskites. *Adv. Mater.* **23**, 4007-4034 (2011).

11 Varghese, J., Whatmore, R. W. & Holmes, J. D. Ferroelectric nanoparticles, wires and tubes: synthesis, characterisation and applications. *J. Mater. Chem. C* **1**, 2618-2638 (2013).

12 Wang, K. *et al.* The Mechanism of Piezocatalysis: Energy Band Theory or Screening Charge Effect? *Angew. Chem. Int. Ed.* **61**, e202110429 (2021).

13 Jiang, Z., Xiao, Z., Tao, Z., Zhang, X. & Lin, S. A significant enhancement of bulk charge separation in photoelectrocatalysis by ferroelectric polarization induced in $CdS/BaTiO_3$ nanowires. *RSC Adv.* **11**, 26534-26545 (2021).

14 Kakekhani, A. & Ismail-Beigi, S. Ferroelectric oxide surface chemistry: water splitting via pyroelectricity. *J. Mater. Chem. A* **4**, 5235-5246 (2016).

15 Kakekhani, A. & Ismail-Beigi, S. Ferroelectric-based catalysis: Switchable surface chemistry. *ACS Catal.* **5**, 4537-4545 (2015).

16 Elmahgary, M. G., Mahran, A. M., Ganoub, M. & Abdellatif, S. O. Optical investigation and computational modelling of $BaTiO_3$ for optoelectronic devices applications. *Sci. Rep.* **13**, 4761 (2023).

17 Qiao, Z., Wang, C., Zou, Y., Wu, X. & Liu, Z. Oxygen vacancy and pyroelectric polarization collaboratively enhancing PEC performance in $BaTiO_3$ photoelectrodes. *Colloids Surf., A* **647**, 129073 (2022).

18 Shi, J. *et al.* Hydrogenated $LaFeO_3$ with oxygen vacancies for enhanced visible light photocatalytic performance. *Ceramics International* **46**, 5315-5322 (2020).

19 Wang, S. *et al.* Enhanced photoelectrochemical performance in $BiFeO_3$/g-C_3N_4 p–n heterojunction photocathodes with ferroelectric polarization. *J. Appl. Phys.* **128**, 154101 (2020).

20 Wang, Z. *et al.* Manipulation of charge transfer and transport in plasmonic-ferroelectric hybrids for photoelectrochemical applications. *Nat. Commun.* **7**, 10348 (2016).

21 Xie, J. *et al.* Bi-functional ferroelectric $BiFeO_3$ passivated $BiVO_4$ photoanode for efficient and stable solar water oxidation. *Nano Energy* **31**, 28-36 (2017).

22 Li, Y., Li, J., Yang, W. & Wang, X. Implementation of ferroelectric materials in photocatalytic and photoelectrochemical water splitting. *Nanoscale Horiz.* **5**, 1174-1187 (2020).

23 Yu, L. *et al.* Recent advances in ferroelectric materials-based photoelectrochemical reaction. *Nanomaterials* **12**, 3026 (2022).
24 Kim, S., Nguyen, N. T. & Bark, C. W. Ferroelectric materials: a novel pathway for efficient solar water splitting. *Appl. Sci.* **8**, 1526 (2018).
25 Kumar, M., Meena, B., Subramanyam, P., Suryakala, D. & Subrahmanyam, C. Recent trends in photoelectrochemical water splitting: the role of cocatalysts. *NPG Asia Materials* **14**, 88 (2022).
26 Toe, C. Y. *et al.* Recent advances and the design criteria of metal sulfide photocathodes and photoanodes for photoelectrocatalysis. *J. Mater. Chem. A* **9**, 20277-20319 (2021).
27 Bharathkumar, S., Sakar, M., Ponpandian, N. & Balakumar, S. Dual oxidation state induced oxygen vacancies in Pr substituted $BiFeO_3$ compounds: An effective material activation strategy to enhance the magnetic and visible light-driven photocatalytic properties. *Mater. Res. Bull.* **101**, 107-115 (2018).
28 Wang, S. *et al.* Hydrogenation-induced surface oxygen vacancies in $BiFeO_3$ nanoparticles for enhanced visible light photocatalytic performance. *J. Alloys Compd.* **688**, 399-406 (2016).
29 Zhang, M. *et al.* Ferroelectric polarization-enhanced charge separation in quantum dots sensitized semiconductor hybrid for photoelectrochemical hydrogen production. *Nano Energy* **81**, 105626 (2021).
30 Zhang, C. *et al.* Hydrogen-treated $BiFeO_3$ nanoparticles with enhanced photoelectrochemical performance. *RSC Adv.* **6**, 24760 (2016).
31 Xiao, M., Luo, B., Wang, Z., Wang, S. & Wang, L. Recent advances of metal-oxide photoanodes: Engineering of charge separation and transportation toward efficient solar water splitting. *Sol. RRL* **4**, 1900509 (2020).
32 Zhou, T. *et al.* Blackened nanostructured $BaTiO_3$ and heterojunction with g-C_3N_4 for enhancing photocatalytic and photoelectrochemical properties. *Mater. Lett.* **342**, 134248 (2023).
33 Djatoubai, E., Khan, M. S., Haq, S. U., Guo, P. & Shen, S. Rational design of $BiFeO_3$ nanostructures for efficient charge carrier transfer and consumption for photocatalytic water oxidation. *J. Alloys Compd.* **911**, 164920 (2022).
34 Andrei, F. *et al.* Thickness-dependent photoelectrochemical water splitting properties of self-assembled nanostructured $LaFeO_3$ perovskite thin films. *Nanomaterials* **11**, 1371 (2021).
35 Singh, S. & Khare, N. Electrically tuned photoelectrochemical properties of ferroelectric nanostructure $NaNbO_3$ films. *Appl. Phys. Lett.* **110**, 152902 (2017).
36 Haydous, F. *et al.* Rolling dopant and strain in Y-doped $BiFeO_3$ epitaxial thin films for photoelectrochemical water splitting. *Sci. Rep.* **8**, 15826 (2018).
37 Wang, J. L., Vilquin, B. & Barrett, N. Screening of ferroelectric domains on $BaTiO_3$(001) surface by ultraviolet photo-induced charge and dissociative water adsorption. *Appl. Phys. Lett.* **101**, 092902 (2012).
38 Yang, Z., Zhao, L., Zhang, S. & Zhao, X. Ferroelectric-enhanced $BiVO_4$ -$BiFeO_3$ photoelectrocatalysis for efficient, stable and large-current-density oxygen evolution. *Appl. Mater.* **26**, 101374 (2022).
39 Zhu, J. *et al.* $BiFeO_3$/Cu_2O heterojunction for efficient photoelectrochemical water splitting under visible-light irradiation. *Catal. Lett.* **151**, 382-389 (2021).
40 Gao, W. *et al.* Industrial carbon dioxide capture and utilization: state of the art and future challenges. *Chem. Soc. Rev.* **49**, 8584-8686 (2020).
41 Liu, R., Zheng, Z., Spurgeon, J. & Yang, X. Enhanced photoelectrochemical water-splitting performance of semiconductors by surface passivation layers. *Energy Environ. Sci.* **7**, 2504-2517 (2014).
42 Sheng, X., Xu, T. & Feng, X. Rational design of photoelectrodes with rapid charge transport for photoelectrochemical applications. *Adv. Mater.* **31**, 1805132 (2019).

43 Chang, X., Wang, T., Yang, P., Zhang, G. & Gong, J. The development of cocatalysts for photoelectrochemical CO_2 reduction. *Adv. Mater.* **31**, 1804710 (2019).

44 Suryawanshi, M. P. *et al.* Earth-abundant photoelectrodes for water splitting and alternate oxidation reactions: Recent advances and future perspectives. *Prog. Mater. Sci.* **134**, 101073 (2023).

45 Sima, M. *et al.* Effect of ferroelectric poling on the photoelectrochemical activity of hematite-$BaTiO_3$ nanowire arrays. *Int. J. Hydrogen Energy* **46**, 36232-36244 (2021).

46 Cui, Y., Briscoe, J. & Dunn, S. Effect of ferroelectricity on solar-light-driven photocatalytic activity of $BaTiO_3$—Influence on the carrier separation and stern layer formation. *Chem. Mater.* **25**, 4215-4223 (2013).

47 Zhao, K., Ouyang, B. & Yang, Y. Enhancing photocurrent of radially polarized ferroelectric $BaTiO_3$ materials by ferro-pyro-phototronic effect. *iScience* **3**, 208-216 (2018).

48 Xu, Q., Berardan, D., Brisset, F., Colbeau-Justin, C. & Ghazzal, M. N. Engineering directional charge carrier transport using ferroelectric polarization for enhanced photoelectrochemical water oxidation. *Small* **20**, 2308750 (2024).

49 Tang, X. & Kou, L. Two-dimensional ferroics and multiferroics: Platforms for new physics and applications. *J. Phys. Chem. Lett.* **10**, 6634-6649 (2019).

50 Wan, T. L. *et al.* Catalysis based on ferroelectrics: controllable chemical reaction with boosted efficiency. *Nanoscale* **13**, 7096-7107 (2021).

51 Augurio, A. *et al.* Controlled Porosity in Ferroelectric $BaTiO_3$ Photoanodes. *ACS Appl. Mater. Interfaces* **14**, 13147–13157 (2022).

52 Khan, M. A., Nadeem, M. A. & Idriss, H. Ferroelectric polarization effect on surface chemistry and photo-catalytic activity: A review. *Surf. Sci. Rep.* **71**, 1-31 (2016).

53 Huang, B. C. *et al.* Direct observation of ferroelectric polarization-modulated band bending at oxide interfaces *Appl. Phys. Lett.* **100**, 122903 (2012).

54 Rioult, M. *et al.* Tailoring the photocurrent in $BaTiO_3$/Nb:$SrTiO_3$ photoanodes by controlled ferroelectric polarization. *Appl. Phys. Lett.* **107**, 103901 (2015).

55 Huang, X. *et al.* Enhanced charge carrier separation to improve hydrogen production efficiency by ferroelectric spontaneous polarization electric field. *Appl. Catal., B* **227**, 322-329 (2018).

56 He, Y. *et al.* Integrated heterostructure of PZT/CdS containing the synergistic effect between heterojunction structure and ferroelectric polarization for photoelectrochemical applications. *Mater. Sci. Semicond. Process.* **121**, 105351 (2021).

57 Tang, X., Shang, J., Gu, Y., Du, A. & Kou, L. Reversible gas capture using a ferroelectric switch and 2D molecule multiferroics on the In_2Se_3 monolayer. *J. Mater. Chem. A* **8**, 7331-7338 (2020).

58 Yun, Y. & Altman, E. I. Using ferroelectric poling to change adsorption on oxide surfaces. *J. Am. Chem. Soc.* **129**, 15684-15689 (2007).

59 Garra, J., Vohs, J. M. & Bonnell, D. A. The effect of ferroelectric polarization on the interaction of water and methanol with the surface of $LiNbO_3$ (0001). *Surf. Sci.* **603**, 1106-1114 (2009).

60 Bhide, V. G., Deshmukh, K. G. & Hegde, M. S. Ferroelectric properties of $PbTiO_3$. *Physica* **28**, 871-876 (1962).

61 Krishna, K. M., Sharon, M. & Mishra, M. K. Preparation and characterization of a $PbTiO_3$ + PbO mixed-oxide photoelectrode. *J. Electroanal. Chem.* **391**, 93-99 (1995).

62 Chao, C. *et al.* Self-templated synthesis of single-crystal and single-domain ferroelectric nanoplates. *Angew. Chem. Int. Ed.* **51**, 9283-9287 (2012).

63 Zhen, C., Ren, Z., Kang, Y., Wang, L. & Liu, G. $PbTiO_3$ based single-domain ferroelectric photocatalysts for water splitting. *Acc. Mater. Res.*, 591–603 (2023).

64 Chao, C., Zhou, Y., Li, H., He, W. & Fa, W. Polarization-induced selective growth of Au islands on single-domain ferroelectric $PbTiO_3$ nanoplates with enhanced photocatalytic activity. *Appl. Surf. Sci.* **466**, 274-281 (2019).

65 Ahn, C. W. *et al.* Effective charge separation in site-isolated Pt-nanodot deposited $PbTiO_3$ nanotube arrays for enhanced photoelectrochemical water splitting. *Appl. Catal., B* **224**, 804-809 (2018).

66 Hu, Y., Dong, W., Zheng, F., Fang, L. & Shen, M. Fe(III) doped and grafted $PbTiO_3$ film photocathode with enhanced photoactivity for hydrogen production. *Appl. Phys. Lett.* **105**, 082903 (2014).

67 Liu, J. *et al.* Impact of alternating current electric field poling on piezoelectric and dielectric properties of $Pb(In_{1/2}Nb_{1/2})O_3$–$Pb(Mg_{1/3}Nb_{2/3})O_3$–$PbTiO_3$ ferroelectric crystals. *J. Appl. Phys.* **128**, 094104 (2020).

68 Xu, J. *et al.* Piezoelectric performance enhancement of $Pb(Mg_{1/3}Nb_{2/3})O_3$-0.25$PbTiO^3$ crystals by alternating current polarization for ultrasonic transducer. *Appl. Phys. Lett.* **112**, 182901 (2018).

69 Jang, J. S. *et al.* Vertically aligned core–shell $PbTiO_3$@TiO_2 heterojunction nanotube array for photoelectrochemical and photocatalytic applications. *J. Phys. Chem. C.* **121**, 15063-15070 (2017).

70 Assavachin, S. & Osterloh, F. E. Ferroelectric polarization in $BaTiO_3$ nanocrystals controls photoelectrochemical water oxidation and photocatalytic hydrogen evolution. *J. Am. Chem. Soc.* **145**, 18825–18833 (2023).

71 Zhao, Y. *et al.* Boosting charge mediation in ferroelectric $BaTiO_{3-x}$-based photoanode for efficient and stable photoelectrochemical water oxidation. *Small*, 2300072 (2023).

72 Yang, W. *et al.* Ferroelectric polarization-enhanced photoelectrochemical water splitting in TiO_2–$BaTiO_3$ core–shell nanowire photoanodes. *Nano Lett.* **15**, 7574-7580 (2015).

73 Magnan, H. *et al.* Tuning the charge carriers migration in epitaxial $BaTiO_3$ thin-film photoanodes. *J. Phys. Chem. C.* **124**, 10315-10323 (2020).

74 Li, X., Bai, Y., Wang, B. C. & Su, Y. J. Water adsorption induced in-plane domain switching on $BaTiO_3$ surface. *J. Appl. Phys.* **118**, 094104 (2015).

75 Huang, Y.-L. *et al.* Tunable photoelectrochemical performance of Au/$BiFeO_3$ heterostructure. *Nanoscale* **8**, 15795-15801 (2016).

76 Yang, S., Ma, G., Xu, L., Deng, C. & Wang, X. Improved ferroelectric properties and band-gap tuning in $BiFeO_3$ films via substitution of Mn. *RSC Adv.* **9**, 29238 (2019).

77 Soltani, T. & Lee, B.-K. Ag-doped $BiVO_4$/$BiFeO_3$ photoanode for highly efficient and stable photocatalytic and photoelectrochemical water splitting. *Sci. Total Environ.* **736**, 138640 (2020).

78 Das, R., Sharma, S. & Mandal, K. Aliovalent Ba^{2+} doping: A way to reduce oxygen vacancy in multiferroic $BiFeO_3$. *Journal of Magnetism and Magnetic Materials* **401**, 129-137 (2016).

79 Schrade, M., Masó, N., Perejón, A., Pérez-Maqueda, L. A. & West, A. R. Defect chemistry and electrical properties of $BiFeO_3$. *J. Mater. Chem. C* **5**, 10077-10086 (2017).

80 Song, J. *et al.* Domain-engineered $BiFeO_3$ thin-film photoanodes for highly enhanced ferroelectric solar water splitting. *Nano Res.* **11**, 642-655 (2018).

81 Singh, S. & Khare, N. Flexible PVDF/Cu/PVDF-$NaNbO_3$ photoanode with ferroelectric properties: An efficient tuning of photoelectrochemical water splitting with electric field polarization and piezophototronic effect. *Nano Energy* **42**, 173-180 (2017).

82 Gómez-Solís, C., Ballesteros, J. C., Torres-Martínez, L. M. & Juárez-Ramírez, I. RuO_2–$NaTaO_3$ heterostructure for its application in photoelectrochemical water splitting under simulated sunlight illumination. *Fuel* **166**, 36-41 (2016).

83 Paulauskas, I. E. *et al.* Growth, characterization, and electrochemical properties of doped n-type $KTaO_3$ photoanodes. *J. Electrochem. Soc.* **156**, B580 (2009).

84 Hu, C.-C., Tsai, C.-C. & Teng, H. Structure characterization and tuning of perovskite-like $NaTaO_3$ for applications in photoluminescence and photocatalysis. *J. Am. Ceram. Soc* **92**, 460-466 (2009).
85 Sun, Z. *et al.* Progress, outlook, and challenges in lead-free energy-storage ferroelectrics. *Adv. Electron. Mater.* **6**, 1900698 (2020).
86 Jin, L., Li, F. & Zhang, S. Decoding the fingerprint of ferroelectric loops: Comprehension of the material properties and structures. *J. Am. Ceram. Soc* **97**, 1-27 (2014).
87 Chen, Z., Dinh, H. N. & Miller, E. *Photoelectrochemical water splitting: Standards, experimental methods, and protocols*. (Springer, 2013).
88 He, J. *et al.* Boosting photocatalytic water oxidation on photocatalysts with ferroelectric single domains. *Adv. Mater.* **35**, 2210374 (2023).
89 Jang, H. W. *et al.* Domain engineering for enhanced ferroelectric properties of epitaxial (001) $BiFeO_3$ thin films. *Adv. Mater.* **21**, 817-823 (2009).
90 Zhang, Q., Valanoor, N. & Standard, O. Epitaxial (001) $BiFeO_3$ thin-films with excellent ferroelectric properties by chemical solution deposition-the role of gelation. *J. Mater. Chem. C* **3**, 582 (2015).
91 Wang, S., Liu, G. & Wang, L. Crystal facet engineering of photoelectrodes for photoelectrochemical water splitting. *Chem. Rev.* **119**, 5192-5247 (2019).
92 Pan, J., Liu, G., Lu, G. Q. M. & Cheng, H.-M. On the true photoreactivity order of {001}, {010}, and {101} facets of anatase TiO_2 crystals. *Angew. Chem., Int. Ed.* **50**, 2133-2137 (2011).
93 Tan, H. L., Amal, R. & Ng, Y. H. Alternative strategies in improving the photocatalytic and photoelectrochemical activities of visible light-driven $BiVO_4$: a review. *J. Mater. Chem. A* **5**, 16498 (2017).
94 Wang, C. *et al.* Facet engineering of advanced electrocatalysts toward hydrogen/oxygen evolution reactions. *Nano-Micro Lett.* **15**, 52 (2023).
95 Zhang, T. *et al.* Insights into the structure–photoreactivity relationships in well-defined perovskite ferroelectric $KNbO_3$ nanowires. *Chem. Sci.* **6**, 4118-4123 (2015).
96 Nagarajan, V. *et al.* Dynamics of ferroelastic domains in ferroelectric thin films. *Nat. Mater.* **2**, 43-47 (2002).
97 Zednik, R. J., Varatharajan, A., Oliver, M., Valanoor, N. & McIntyre, P. C. Mobile ferroelastic domain walls in nanocrystalline PZT films: the direct piezoelectric effect. *Adv. Funct. Mater.* **21**, 3104-3110 (2011).
98 Nagarajan, V. *et al.* Realizing intrinsic piezoresponse in epitaxial submicron lead zirconate titanate capacitors on Si *Appl. Phys. Lett.* **81**, 4215–4217 (2002).
99 Shi, Q. *et al.* The role of lattice dynamics in ferroelectric switching. *Nat. Commun.* **13**, 1110 (2022).
100 Cruz, J. P. d. l., Joanni, E., Vilarinho, P. M. & Kholkin, A. L. Thickness effect on the dielectric, ferroelectric, and piezoelectric properties of ferroelectric lead zirconate titanate thin films. *J. Appl. Phys.* **108**, 114106 (2010).
101 Wang, J. *et al.* Epitaxial $BiFeO_3$ multiferroic thin film heterostructures. *Science* **299**, 1719-1722 (2003).
102 Singh, A., Khan, Z. R., Vilarinho, P. M., Gupta, V. & Katiyar, R. S. Influence of thickness on optical and structural properties of BiFeO3 thin films: PLD grown. *Materials Research Bulletin* **49**, 531-536 (2014). https://doi.org/https://doi.org/10.1016/j.materresbull.2013.08.050
103 Qiu, C., Liu, J., Li, F. & Xu, Z. Thickness dependence of dielectric and piezoelectric properties for alternating current electric-field-poled relaxor-$PbTiO_3$ crystals. *J. Appl. Phys.* **125**, 014102 (2019).
104 Liu, Q. *et al.* Enhanced ferroelectric photoelectrochemical properties of polycrystalline $BiFeO_3$ film by decorating with Ag nanoparticles. *Appl. Phys. Lett.* **108**, 022902 (2016).
105 Low, J., Yu, J., Jaroniec, M., Wageh, S. & Al-Ghamdi, A. A. Heterojunction photocatalysts. *Adv. Mater.* **29**, 1601694 (2017).

106 Afroz, K., Moniruddin, M., Bakranov, N., Kudaibergenov, S. & Nuraje, N. A heterojunction strategy to improve the visible light sensitive water splitting performance of photocatalytic materials. *J. Mater. Chem. A* **6**, 21696-21718 (2018).

107 Huang, J. *et al.* Synergistically enhanced charge separation in $BiFeO_3$/Sn:TiO_2 nanorod photoanode via bulk and surface dual modifications *Nano Energy* **59**, 33-40 (2019).

108 Kamat, P. V. Meeting the clean energy demand: Nanostructure architectures for solar energy conversion. *J. Phys. Chem. C.* **111**, 2834-2860 (2007).

109 Li, S., Xu, W., Meng, L., Tian, W. & Li, L. Recent progress on semiconductor heterojunction-based photoanodes for photoelectrochemical water splitting. *Small Science* **2**, 2100112 (2022).

110 Oshime, N. *et al.* Skewed electronic band structure induced by electric polarization in ferroelectric $BaTiO_3$. *Scientific Reports* **10**, 10702 (2020).

111 Chen, Y. *et al.* Ferroelectric-tuned van der Waals heterojunction with band alignment evolution. *Nat. Commun.* **12**, 4030 (2021).

112 Parangusan, H. *et al.* Hierarchical $BaTiO_3$/$NiFe_2O_4$ nanocomposite as an efficacious photoanode for photoelectrochemical water splitting. *Ceramics International* **48**, 29136-29143 (2022).

113 Wu, F. *et al.* Simultaneous enhancement of charge separation and hole transportation in a TiO_2–$SrTiO_3$ core–shell nanowire photoelectrochemical system. *Adv. Mater.* **29**, 1701432 (2017).

114 Wu, X. *et al.* Ferroelectric enhanced photoelectrochemical water splitting in $BiFeO_3$/TiO_2 composite photoanode. *J. Alloys Compd.* **783**, 643-651 (2019).

115 Gunawan, M. *et al.* [Pre-print] Ferroelectric polarization-induced performance enhancements in $BiFeO_3$-based photoanodes for photoelectrochemical water splitting (2024).

116 Khoomortezaei, S., Abdizadeh, H. & Golobostanfard, M. R. Triple Layer Heterojunction WO_3/$BiVO_4$/$BiFeO_3$ Porous Photoanode for Efficient Photoelectrochemical Water Splitting. *ACS Applied Energy Materials* **2**, 6428-6439 (2019). https://doi.org/10.1021/acsaem.9b01041

117 Khoomortezaei, S., Abdizadeh, H. & Golobostanfard, M. R. Ferro-photocatalytic enhancement of photoelectrochemical water splitting using the WO_3/$BiFeO_3$ heterojunction. *Energy Fuels* **35**, 9623-9634 (2021).

118 Wang, M. *et al.* Improving the charge properties of the WO3 photoanode using a $BiFeO_3$ ferroelectric nanolayer. *Phys. Chem. Chem. Phys.* **23**, 8241-8245 (2021).

119 Koyyada, G. *et al.* $BiFeO_3$/Fe_2O_3 electrode for photoelectrochemical water oxidation and photocatalytic dye degradation: A single step synthetic approach. *Chemosphere* **303**, 135071 (2022).

120 Fang, T. *et al.* Type-II band alignment enhances unassisted photoelectrochemical water-splitting performance of the $BaTiO_3$/CdS ferroelectric heterostructure photoanode under solar light irradiation. *J. Phys. Chem. C.* **125**, 18734-18742 (2021).

121 Farooq, U. *et al.* Development of heterostructured ferroelectric $SrZrO_3$/CdS photocatalysts with enhanced surface area and photocatalytic activity. *J. Nanosci. Nanotechnol.* **20**, 3770-3779 (2020).

122 Zou, X., Sun, Z. & Hu, Y. H. g-C_3N_4-based photoelectrodes for photoelectrochemical water splitting: a review. *J. Mater. Chem. A* **8**, 21474-21502 (2020).

123 Gopalakrishnan, S., Bhalerao, G. M. & Jeganathan, K. $SrTiO_3$ NPs/g-C_3N_4 NSs coupled Si NWs based hybrid photocathode for visible light driven photoelectrochemical water reduction. *ACS Sustainable Chem. Eng.* **7**, 13911-13919 (2019).

124 Yang, M.-Q., Wang, J., Wu, H. & Ho, G. W. Noble metal-free nanocatalysts with vacancies for electrochemical water splitting. *Small* **14**, 1703323 (2018).

125 Ding, C., Shi, J., Wang, Z. & Li, C. Photoelectrocatalytic water splitting: significance of cocatalysts, electrolyte, and interfaces. *ACS catalysis* **7**, 675-688 (2017).
126 Wang, Z., Lin, R., Huo, Y., Li, H. & Wang, L. Formation, detection, and function of oxygen vacancy in metal oxides for solar energy conversion. *Adv. Funct. Mater.* **32**, 2109503 (2022).
127 Ding, J. *et al.* Bandgap engineering strategy through chemical strain and oxygen vacancies in super-tetragonal $BiFeO_3$ epitaxial films. *Inorg. Chem. Front.* **10**, 1215-1224 (2023).
128 Yang, T. *et al.* Design of oxygen vacancy in $BiFeO_3$-based films for higher photovoltaic performance. *Appl. Surf. Sci.* **575**, 151713 (2022).
129 Chen, D. *et al.* Defective $BiFeO_3$ with surface oxygen vacancies: Facile synthesis and mechanism insight into photocatalytic performance. *Solar Energy Materials and Solar Cells* **171**, 24-32 (2017).
130 Chen, L. *et al.* First direct observation of the built-in electric field and oxygen vacancy migration in ferroelectric $Hf_{0.5}Zr_{0.5}O_2$ film during electrical cycling. *Nanoscale* **15**, 7014-7022 (2023).
131 Yu, H. *et al.* Synergy of ferroelectric polarization and oxygen vacancy to promote CO_2 photoreduction. *Nat. Commun.* **12**, 4594 (2021).
132 Dalton, P. D. *et al.* Electrospinning and additive manufacturing: converging technologies. *Biomater. Sci.* **1**, 171-185 (2013).
133 Xu, Q. *et al.* The role of Bi vacancies in the electrical conduction of $BiFeO_3$: a first-principles approach. *Dalton Trans.* **43**, 10787-10793 (2014).
134 Sun, Y. *et al.* Insight into the enhanced photoelectrocatalytic activity in reduced $LaFeO_3$ films. *Chem. Commun.* **53**, 2499-2502 (2017).
135 Radmilovic, A., Smart, T. J., Ping, Y. & Choi, K.-S. Combined experimental and theoretical investigations of n-type $BiFeO_3$ for use as a photoanode in a photoelectrochemical cell. *Chem. Mater.* **32**, 3262-3270 (2020).
136 Prasad, N. P. *et al.* Role of excess Bi on the properties and performance of $BiFeO_3$ thin-film photocathodes. *ACS Appl. Energy Mater.* **6**, 12237–12248 (2023).
137 Lee, D. *et al.* Emergence of room-temperature ferroelectricity at reduced dimensions. *Science* **349**, 1314-1317 (2015).
138 Li, W., Shi, J., Zhang, K. H. L. & MacManus-Driscoll, J. L. Defects in complex oxide thin films for electronics and energy applications: challenges and opportunities. *Mater. Horiz.* **7**, 2832-2859 (2020).
139 Tran-Phu, T. *et al.* Understanding the role of vanadium vacancies in $BiVO_4$ for efficient photoelectrochemical water oxidation. *Chem. Mater.* **33**, 3553–3565 (2021).
140 Schiemer, J. A., Withers, R. L., Liu, Y. & Carpenter, M. A. Ca-doping of $BiFeO_3$: The role of strain in determining coupling between ferroelectric displacements, magnetic moments, octahedral tilting, and oxygen-vacancy ordering. *Chem. Mater.* **25**, 4436-4446 (2013).
141 Singh, S., Sangle, A. L., Wu, T., Khare, N. & MacManus-Driscoll, J. L. Growth of doped $SrTiO_3$ ferroelectric nanoporous thin films and tuning of photoelectrochemical properties with switchable ferroelectric polarization. *ACS Appl. Mater. Interfaces* **11**, 45683-45691 (2019).
142 Gupta, T., Samriti, Cho, J. & Prakash, J. Hydrothermal synthesis of TiO_2 nanorods: Formation chemistry, growth mechanism, and tailoring of surface properties for photocatalytic activities. *Mater. Today Chem.* **20**, 100428 (2021).
143 Lee, H. J., Shin, S.-H., Nam, K. T., Nah, J. & Lee, M. H. Spontaneously polarized lithium-doped zinc oxide nanowires as photoanodes for electrical water splitting. *J. Mater. Chem. A* **4**, 3223-3227 (2016).
144 Cheng, X., Zhang, Y., Hu, H., Shang, M. & Bi, Y. High-efficiency $SrTiO_3/TiO_2$ hetero-photoanode for visible-light water splitting by charge transport design and optical absorption management. *Nanoscale* **10**, 3644-3649 (2018).
145 Zhang, Q., Sando, D. & Nagarajan, V. Chemical route derived bismuth ferrite thin films and nanomaterials. *Journal of Materials Chemistry C* **4** (2016).

146 Qin, M., Yao, K. & Liang, Y. C. Photovoltaic characteristics in polycrystalline and epitaxial $(Pb_{0.97}La_{0.03})(Zr_{0.52}Ti_{0.48})O_3$ ferroelectric thin films sandwiched between different top and bottom electrodes. *J. Appl. Phys.* **105**, 061624 (2009).

147 Mazet, L., Yang, S. M., Kalinin, S. V., Schamm-Chardon, S. & Dubourdieu, C. A review of molecular beam epitaxy of ferroelectric $BaTiO_3$ films on Si, Ge and GaAs substrates and their applications. *Sci. Technol. Adv. Mater.* **16**, 036005 (2015).

148 Fernandez, A. *et al.* Thin-film ferroelectrics. *Adv. Mater.* **34**, 2108841 (2022).

149 Moniz, S. J. A. *et al.* A simple, low-cost CVD route to thin films of $BiFeO_3$ for efficient water photo-oxidation. *J. Mater. Chem. A* **2**, 2922-2927 (2014).

150 Wei, Z., Yao, Y., Huang, T. & Yu, A. Solvothermal growth of well-aligned TiO_2 nanowire arrays for dye-sensitized solar cell: Dependence of morphology and vertical orientation upon substrate pretreatment. *Int. J. Electrochem. Sci.* **6**, 1871 - 1879 (2011).

151 Zheng, F., Lu, H., Guo, M. & Zhang, M. Effect of substrate pre-treatment on controllable synthesis of hexagonal WO_3 nanorod arrays and their electrochromic properties. *CrystEngComm* **15**, 5828-5837 (2013).

152 Dani, S. S., Tripathy, A., Alluri, N. R., Balasubramaniam, S. & Ramadoss, A. A critical review: the impact of electrical poling on the longitudinal piezoelectric strain coefficient. *Mater. Adv.* **3**, 8886-8921 (2022).

153 Hartono, A. *et al.* Electric field poling 2G V/m to improve piezoelectricity of PVDF thin film. *AIP Conference Proceedings* **1719**, 030021 (2016).

154 Fan, G., Lu, W., Wang, X. & Liang, F. Morphotropic phase boundary and piezoelectric properties of $(Bi_{1/2}Na_{1/2})TiO_3$–$(Bi_{1/2}K_{1/2})TiO_3$–$KNbO_3$ lead-free piezoelectric ceramics. *Appl. Phys. Lett.* **91**, 202908 (2007).

155 Park, C., Ounaies, Z., Wise, K. E. & Harrison, J. S. In situ poling and imidization of amorphous piezoelectric polyimides. *Polymer* **45**, 5417-5425 (2004).

156 Bhardwaj, N. & Kundu, S. C. Electrospinning: A fascinating fiber fabrication technique. *Biotechnology Advances* **28**, 325-347 (2010).

157 Tanahashi, I., Manabe, Y., Tohda, T., Sasaki, S. & Nakamura, A. Optical nonlinearities of Au/SiO_2 composite thin films prepared by a sputtering method. *J. Appl. Phys.* **79**, 1244-1249 (1996).

158 Garrett, M. H., Chang, J. Y., Jenssen, H. P. & Warde, C. A method for poling barium titanate, $BaTiO_3$. *Ferroelectrics* **120**, 167-173 (1991).

159 Kim, H. *et al.* Increased piezoelectric response in functional nanocomposites through multiwall carbon nanotube interface and fused-deposition modeling three-dimensional printing. *MRS Communications* **7**, 960-966 (2017).

160 Weinberg, Z. A., Johnson, W. C. & Lampert, M. A. High-field transport in SiO_2 on silicon induced by corona charging of the unmetallized surface. *J. Appl. Phys.* **47**, 248-255 (1976).

161 Rotan, M., Zhuk, M. & Glaum, J. Activation of ferroelectric implant ceramics by corona discharge poling. *J. Eur. Ceram. Soc.* **40**, 5402-5409 (2020).

162 Cao, D. *et al.* Switchable charge-transfer in the photoelectrochemical energy-conversion process of ferroelectric $BiFeO_3$ photoelectrodes. *Angew. Chem., Int. Ed.* **53**, 11027-11031 (2014).

163 Liu, Z. *et al.* Piezoelectric-effect-enhanced full-spectrum photoelectrocatalysis in p–n heterojunction. *Adv. Funct. Mater.* **29**, 1807279 (2019).

164 Cao, D. *et al.* Understanding the nature of remnant polarization enhancement, coercive voltage offset and time-dependent photocurrent in ferroelectric films irradiated by ultraviolet light. *J. Mater. Chem.* **22**, 12592-12598 (2012).

165 Chen, X., Liu, C., Hua, Z. & Ma, N. Ferroelectric polarization and oxygen vacancy synergistically induced an ultrasensitive and fast humidity sensor for multifunctional applications. *ACS Appl. Mater. Interfaces* **14**, 49965–49974 (2022).

166 Klyukin, K. & Alexandrov, V. Effect of intrinsic point defects on ferroelectric polarization behavior of $SrTiO_3$. *Phys. Rev. B* **95**, 035301 (2017).
167 Liu, T., Pei, J., Xu, J., Guo, Q. & Li, R. Analysis of PZT/PVDF composites performance reinforced by aramid fibers. *Mater. Res. Express* **6**, 066303 (2019).
168 Ramadan, K. S., Sameoto, D. & Evoy, S. A review of piezoelectric polymers as functional materials for electromechanical transducers. *Smart Mater. Struct.* **23**, 033001 (2014).
169 Njiwa, A. B. K., Aulbach, E., Granzow, T. & Rödel, J. Influence of radial stress on the poling behaviour of lead zirconate titanate ceramics. *Acta Mater.* **55**, 675-680 (2007).
170 Tian, Y. *et al.* Water printing of ferroelectric polarization. *Nat. Commun.* **9**, 3809 (2018).
171 Tian, Z. *et al.* Selective photoelectrochemical oxidation of glucose to glucaric acid by single atom Pt decorated defective TiO_2. *Nat. Commun.* **14**, 142 (2023).
172 Vo, T.-G., Kao, C.-C., Kuo, J.-L., Chiu, C.-c. & Chiang, C.-Y. Unveiling the crystallographic facet dependence of the photoelectrochemical glycerol oxidation on bismuth vanadate. *Applied Catalysis B: Environmental* **278**, 119303 (2020). https://doi.org/https://doi.org/10.1016/j.apcatb.2020.119303
173 Li, L. *et al.* Impact of ferroelectric polarization on different semiconductors for photoelectrochemical application. *ACS Sustainable Chem. Eng.* **7**, 19640-19648 (2019).
174 Zhu, Y. *et al.* Effect of ferroelectric polarization field on different carrier migration in photoanode. *Mater. Sci. Semicond. Process.* **133**, 105958 (2021).
175 Vishwakarma, A. K. *et al.* Synthesis and characterizations of graphene/Sm doped $BiFeO_3$ composites photoanode for efficient photo-electrochemical water splitting. *Int. J. Hydrogen Energy* **46**, 15550-15560 (2021).
176 Liu, Y. *et al.* Ferroelectric polarization-enhanced charge separation in a vanadium-doped ZnO photoelectrochemical system. *Inorg. Chem. Front.* **5**, 1533-1539 (2018).
177 He, X. *et al.* Novel Fe_2O_3/PZT nanorods for ferroelectric polarization-enhanced photoelectrochemical water splitting. *Energy Fuels* **34**, 16927-16935 (2020).
178 Huang, W. *et al.* Epitaxial Bi_2FeCrO_6 multiferroic thin-film photoanodes with ultrathin p-type NiO layers for improved solar water oxidation. *ACS Appl. Mater. Interfaces* **11**, 13185-13193 (2019).
179 Liu, B., Sun, M., Tan, B., Zhang, Z. & Han, W. Enhanced photocarrier collection in bismuth vanadate photoanode through modulating the inner potential distribution. *Adv. Opt. Mater.* **10**, 2200046 (2022).
180 Li, C. *et al.* Synthesis and enhanced bias-free photoelectrochemical water-splitting activity of ferroelectric $BaTiO_3/Cu_2O$ heterostructures under solar light irradiation. *Ceramics International* **47**, 11379-11386 (2021).
181 Wang, S. *et al.* Self-enhancing photoelectrochemical properties in van der waals ferroelectric $CuInP_2S_6$ by photoassisted acid hydrolysis. *ACS Appl. Mater. Interfaces* **14**, 40126-40135 (2022).

View Article Online
DOI: 10.1039/D4TA07812H

Data availability statement

No primary research results, software or code have been included and no new data were generated or analysed as part of this review.